JCB Journal of Cell Biology

ARTICLE

Branched actin networks are assembled on microtubules by adenomatous polyposis coli for targeted membrane protrusion

Nadia Efimova[1], Changsong Yang[1], Jonathan X. Chia[1], Ning Li[2], Christopher J. Lengner[2,3], Kristi L. Neufeld[4], and Tatyana M. Svitkina[1]

Cell migration is driven by pushing and pulling activities of the actin cytoskeleton, but migration directionality is largely controlled by microtubules. This function of microtubules is especially critical for neuron navigation. However, the underlying mechanisms are poorly understood. Here we show that branched actin filament networks, the main pushing machinery in cells, grow directly from microtubule tips toward the leading edge in growth cones of hippocampal neurons. Adenomatous polyposis coli (APC), a protein with both tumor suppressor and cytoskeletal functions, concentrates at the microtubule-branched network interface, whereas APC knockdown nearly eliminates branched actin in growth cones and prevents growth cone recovery after repellent-induced collapse. Conversely, encounters of dynamic APC-positive microtubule tips with the cell edge induce local actin-rich protrusions. Together, we reveal a novel mechanism of cell navigation involving APC-dependent assembly of branched actin networks on microtubule tips.

Introduction

Directional migration of individual cells in multicellular organisms plays key roles in multiple aspects of normal development and disease. The precision with which cells find their destinations is especially critical for neurons, which extend their processes, axons and dendrites, over enormous distances and need to find exact targets in order to establish functional neural circuitry during development and following regeneration after injury. Any imperfection in this daunting task leads to neuropsychiatric disorders (Blanquie and Bradke, 2018; Eira et al., 2016; Engle, 2010; Muñoz-Lasso et al., 2020).

The cytoskeleton is the main cellular machinery that generates force for migration and executes cellular decisions in response to guidance cues. The cytoskeleton components playing major roles in cell motility, microtubules and actin filaments, are responsible for different aspects of cell motility, but also extensively cooperate with each other. The actin cytoskeleton can produce large pushing and pulling forces to drive cell protrusion and contraction, respectively (Svitkina, 2018). Leading edge protrusion is typically driven by polymerizing actin filaments in the form of Arp2/3 complex-dependent branched actin networks. Microtubules, on the other hand, largely function as "managers" by coordinating pushing and pulling activities of the actin cytoskeleton in space and time to enable directional cell migration (Vasiliev et al., 1970) and neuron navigation (Tanaka and Kirschner, 1995). However, it remains poorly understood how microtubules accomplish their "supervising" roles. Besides serving as tracks for the intracellular transport, the best known function of microtubules, microtubules can also manipulate the actin cytoskeleton by regulating Rho family GTPases (Krendel et al., 2002; van Haren et al., 2014) and cell–matrix adhesions (Kaverina et al., 1999), and by inducing assembly of unbranched actin filaments in cooperation with formin family actin nucleators (Henty-Ridilla et al., 2016).

Actin-microtubule cooperation is particularly important in neurons (Cammarata et al., 2016; Pacheco and Gallo, 2016), where such cross-talk ensures precise connectivity in the neural circuitry. Growth cones, the actin-rich structures at the tips of microtubule-rich neurites, drive neurite extension and guide them toward proper targets. Bidirectional actin-microtubule cross-talk plays important roles in growth cone motility (Dogterom and Koenderink, 2019). On one hand, the actin cytoskeleton can regulate the distribution of microtubules. For example, microtubules can be captured and guided to the cell periphery by actin filament bundles in filopodia (Burnette et al.,

[1]Department of Biology, School of Arts and Sciences, University of Pennsylvania, Philadelphia, PA; [2]Department of Biomedical Sciences, School of Veterinary Medicine, University of Pennsylvania, Philadelphia, PA; [3]Department of Cell and Developmental Biology, Perelman School of Medicine and Institute for Regenerative Medicine, University of Pennsylvania, Philadelphia, PA; [4]Department of Molecular Biosciences, University of Kansas, Lawrence, KS.

Correspondence to Tatyana M. Svitkina: svitkina@sas.upenn.edu.

2007; Dent and Kalil, 2001; Schaefer et al., 2002; Zhou et al., 2002) or kept away from the leading edge by the actin retrograde flow (Myers et al., 2006; Schaefer et al., 2002). These phenomena likely require physical interaction between actin filaments and microtubules, which can be mediated, for example, by septins (Hu et al., 2012), doublecortin (Tint et al., 2009), drebrin (Geraldo et al., 2008), and/or spectraplakins (Alves-Silva et al., 2012). On the reverse side, microtubules also can regulate actin dynamics. In striking examples of this kind in neurons, "pioneer" microtubules that approach the growth cone periphery induce growth cone advance or turning (Bearce et al., 2015; Buck and Zheng, 2002; Dent et al., 2003), whereas microtubules entering dendritic spines, actin-rich protrusions that form the postsynaptic component of excitatory synapses, induce spine expansion and synapse strengthening (Hu et al., 2011; Jaworski et al., 2009). Since both growth cone motility and dendritic spine expansion depend on the assembly of the Arp2/3-dependent branched actin networks (Korobova and Svitkina, 2008, 2010), these observations suggest that microtubules may be able to locally induce assembly of branched actin networks. However, this possibility so far remains purely hypothetical, if considered at all.

A starting point for this study was our serendipitous discovery by platinum replica electron microscopy (PREM), a technique uniquely suited for visualization of fine architecture of the cytoskeleton (Svitkina, 2017), that branched actin networks can be physically associated with microtubules in neuronal growth cones, suggesting that a microtubule might be able to directly "tell" the growth cone which way to go. In this study, we investigated the molecular mechanism of microtubule-dependent branched network assembly and uncovered key roles of adenomatous polyposis coli (APC) in this process.

Although best known as a tumor suppressor (Zhang and Shay, 2017), APC is also a cytoskeletal protein that regulates cell motility and polarity (Nelson and Näthke, 2013), as well as neurite outgrowth (Koester et al., 2007; Yokota et al., 2009). APC can interact with the microtubule lattice directly and also bind growing microtubule ends by interacting with end-binding (EB) proteins (Jiang and Akhmanova, 2011; Zumbrunn et al., 2001), the core family of plus-end tracking proteins (+TIPs; Bearce et al., 2015). APC can also bind actin (Moseley et al., 2007) and nucleate unbranched actin filaments, either by itself or in cooperation with formins (Breitsprecher et al., 2012; Okada et al., 2010). These APC interactions depend on the sequences located within the C-terminal region of APC. The central unstructured region of APC is responsible for tumor suppressor functions of APC by binding components of the β-catenin destruction complex (Zhang and Shay, 2017). The N terminus of APC containing Armadillo repeats, among other interaction partners, binds and activates the Cdc42 guanine nucleotide exchange factor, Asef (Kawasaki et al., 2000; Mitin et al., 2007), thus forming a potential link through Cdc42 (Gotthardt and Ahmadian, 2007; Hamann et al., 2007) and its effector N-WASP (Rohatgi et al., 1999) to activation of the Arp2/3 complex and formation of branched actin networks. APC is highly enriched in neuronal tissues (Bhat et al., 1994), whereas APC mutations have been linked to intellectual disabilities and neurological disorders (Gonzalez et al., 2015; Mohn et al., 2014; Onouchi et al., 2014). Therefore, our findings not only uncover a fundamental cell biological mechanism but also shed light on the etiology of some human diseases.

Results

Association of branched actin networks with microtubule tips in neuronal growth cones

We used PREM to study the cytoskeletal structure of growth cones of cultured rat hippocampal neurons (Fig. 1). In PREM images, actin filaments and microtubules can be distinguished by their thickness, which is ~10 nm for actin filaments and ~25 nm for microtubules (including platinum coating), whereas immunogold labeling of microtubules improves detection of microtubules within dense actin networks. Several types of actin filament arrays could physically associate with microtubule tips in neuronal growth cones (Fig. 1, A and I). Specifically, 24.1% of clearly distinguishable microtubule tips were associated with filopodial bundles (Fig. 1 A, green arrowheads), as observed previously (Dent et al., 2007; Schaefer et al., 2002). An identical fraction (24.1%) of tips was associated with individual linear actin filaments that extended from the microtubule into the surrounding actin network (Fig. 1 A, yellow arrowhead). The most striking actin-microtubule arrangement, however, was the association of branched actin filaments with the distal microtubule regions (Fig. 1, A, B, D, F, and H; blue shade), which was seen at 34.5% of microtubule ends (Fig. 1 I). Of these cases, 73.3% (25.3% of total) of branched actin filaments could be clearly traced back to the microtubule surface, whereas in the remaining 26.7% of cases (9.2% of total), microtubule tips ended within a dense local patch of branched actin network (Fig. 1 A, dark blue arrowhead). In 17.2% of cases, microtubules ended within a complex actin network that could not be explicitly categorized. Branched actin networks associating with microtubule tips were also observed in nonneuronal COS7 cells (Fig. S1).

Branched actin networks are generated by the Arp2/3 complex, which nucleates new actin branches on the side of preexisting "mother" actin filaments creating a ~70° angle between the barbed (plus) ends of mother and daughter filaments (Mullins et al., 1998; Svitkina and Borisy, 1999). The orientation of this angle, which corresponds to the direction of applied force, suggested that the actin network grew from the microtubule surface toward the nearest edge (Fig. 1, B, D, and F). The branched networks often sprouted from a few microtubule-associated unbranched actin filaments (Fig. 1, F and H) that appeared to serve as initial mother filaments for branched nucleation. We could occasionally detect additional material at microtubule tips (Fig. 1 F, purple), which likely corresponded to a collection of +TIPs, which mediate many microtubule functions (Bearce et al., 2015). The observed position and geometry of the microtubule-associated branched networks are favorable for driving local plasma membrane protrusion near the microtubule tip.

Availability of mother filaments, which also serve as Arp2/3 complex coactivators (Machesky et al., 1999), may be a rate-limiting

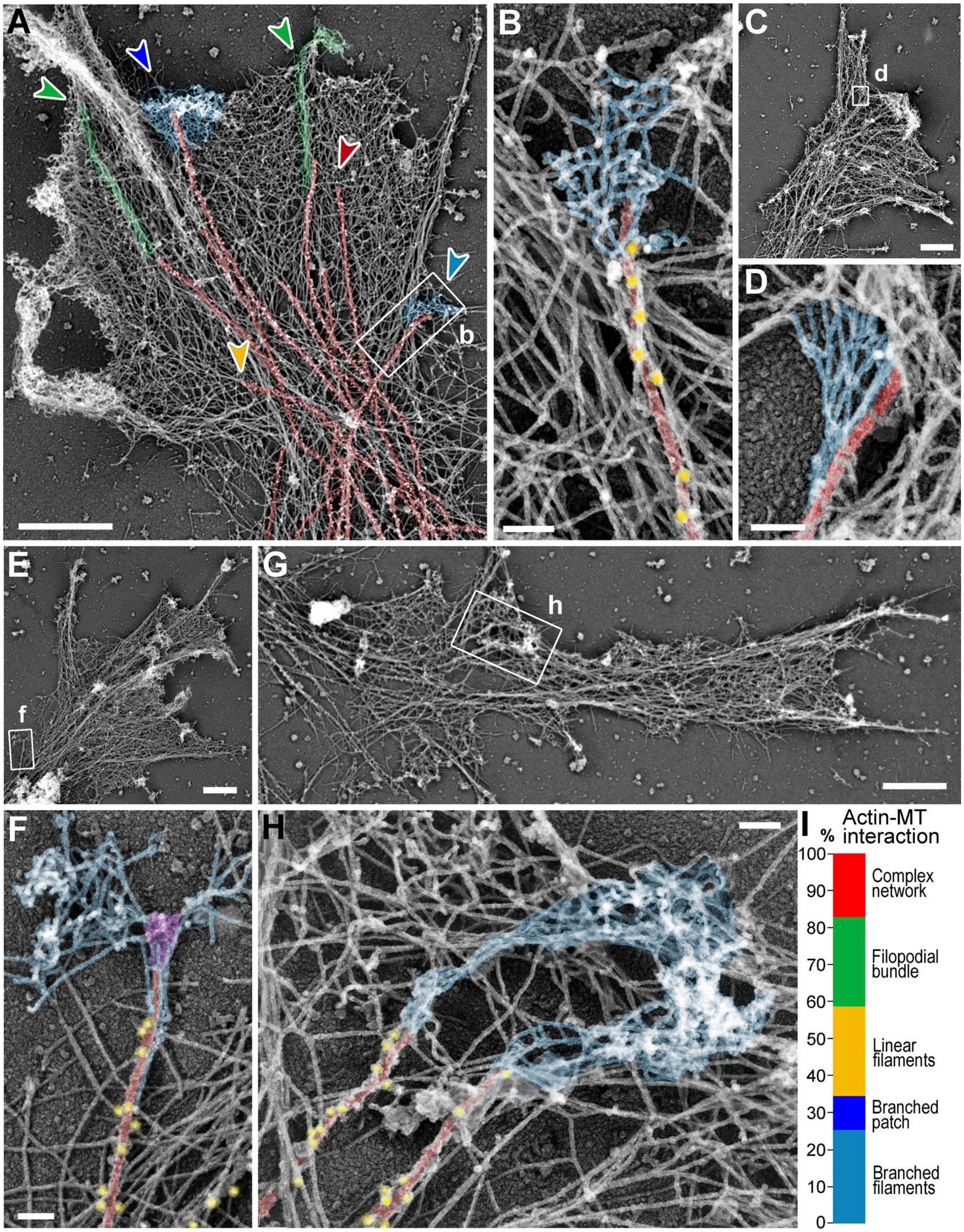

Figure 1. **Branched actin networks in growth cones can be physically linked to MT tips. (A–H)** PREM of growth cones of DIV1 (C and D) or DIV2 (A, B, and E–H) rat hippocampal neurons. Boxed regions in panels A, C, E, and G are enlarged in panels B, D, F, and H, respectively. Color coding: microtubules (red), branched actin networks associated with microtubules (light blue), filopodial bundles (green), α-tubulin immunogold (yellow), and putative +TIPs (purple). **(I)** Percentage of indicated actin filament arrays associated with microtubule ends in growth cones; *n* = 87 microtubules in 15 growth cones from six DIV2 neurons labeled with α-tubulin immunogold; one experiment was quantified; six additional independent experiments with DIV2/3 neurons, either unlabeled (four experiments) or labeled by α-tubulin immunogold (two experiments), were assessed qualitatively. Examples of these arrays are shown in A by arrowheads of matching colors. Scale bars, 1 µm (A, C, E, and G); 100 nm (B, D, F, and H).

step for starting new branched networks. The existence of microtubule-associated branched networks suggests that microtubules may be able to somehow overcome this problem. If so, microtubules are expected to be more extensively employed in this capacity when availability of preexisting actin filaments is decreased, for example, following treatment with actin-depolymerizing drugs. We tested this prediction by culturing hippocampal neurons in the presence of low concentrations (1–5 μM) of cytochalasin D (CytoD) or latrunculin B (LatB), which still permit actin-dependent neurite outgrowth (Chia et al., 2016). PREM analysis revealed the actin-rich growth cone-like structures at the neurite tips of CytoD- or LatB-treated neurons, which contained dense networks of branched actin filaments often associated with microtubules (Fig. 2).

Localization of APC at the interface between microtubules and branched actin networks

Microtubules cannot directly bind or nucleate actin filaments, suggesting that some cross-linkers connect branched actin filaments and microtubules. Among multiple candidates proposed to serve as actin–microtubule cross-linkers (Cammarata et al., 2016; Dogterom and Koenderink, 2019), APC uniquely combines promising biochemical properties (see Introduction) with an ability to regulate neurite outgrowth (Koester et al., 2007; Yokota et al., 2009), which makes it an excellent candidate to initiate the formation of branched actin networks in a microtubule-dependent manner.

In cultured neurons, APC was expressed throughout in vitro development but at slightly higher levels in more mature neurons (Fig. 3 A). By fluorescence microscopy, APC in young neurons cultured for 2 d in vitro (DIV) was often distributed in the form of small scattered puncta, whereas growth cones of mature DIV14 neurons mostly contained bright APC streaks (Fig. 3, B and C). Both types of APC structures colocalized with microtubule ends (Fig. 3 B). In growth cones of young DIV2–3 neurons treated with CytoD or LatB, APC showed prominent clustering analogous to that in untreated mature DIV14 growth cones (Fig. S2, A and B). Interestingly, F-actin in these inhibitor-treated neurons almost perfectly colocalized with APC, suggesting that APC accumulations could promote local actin assembly in conditions of hindered actin assembly.

If APC connects microtubules and branched actin networks, it should localize at the microtubule-actin interface in these structures. Using PREM of DIV3 and DIV14 neurons in combination with APC immunogold labeling (Fig. 4), we indeed detected APC at such interfaces. Consistent with the immunofluorescence data (Fig. 3 B), APC immunogold particles were more abundant at the microtubule-actin junctions in DIV14 growth cones (Fig. 4, E–I) and in DIV3 growth cones of CytoD-treated neurons (Fig. S2, C and D) as compared with untreated DIV3 growth cones (Fig. 4, A–D). APC immunogold particles were also present along the length of microtubules and on actin filaments, as expected based on the ability of APC to bind the microtubule lattice and actin filaments. Notably, the immunogold labeling was specific, because we observed virtually no labeling when we omitted the primary antibody (Fig. S3, A and B). Thus, APC is properly localized to serve as a linker between microtubules and branched actin networks in growth cones.

Induction of local actin-rich protrusions by APC-positive microtubules

Using coexpression of fluorescently tagged APC with either F-tractin, a marker of F-actin, or cortactin, a marker of branched actin networks, in REF52 or COS7 cells, we correlated APC dynamics with actin-based protrusions (Fig. 5, A–C and E; and Fig. S4). As a control, we expressed EGFP-EB3 with F-tractin or cortactin (Fig. 5, D and E). As shown previously (Kita et al., 2006; Mimori-Kiyosue et al., 2000), full-length APC often formed relatively stable accumulations in the vicinity of cell edges. Within these accumulations, individual APC clusters, likely associated with microtubule tips, made relatively short runs toward the cell edge, roamed around within a small area, or remained nearly stationary. During roaming behavior, APC clusters usually remained distant from the cell edge. No obvious correlation between APC motility and cell edge protrusion was observed in such cases. The stationary APC clusters often persisted at the cell edge for the duration of several protrusion-withdrawal cycles of the cell edge, which made these events unsuitable for correlative analysis. However, when an APC cluster hit the cell edge after a detectable run toward the edge, such encounters were often followed by a local F-tractin– or cortactin-rich protrusion (Fig. 5, B and C; Fig. S4; and Videos 1, 2, 3, and 4). Quantification of such events in REF52 cells revealed that 64.1 ± 7.0% of the APC-edge encounters were followed within ∼30 s by a local F-actin–rich or cortactin-rich protrusion, as compared with only 30.1 ± 3.9% of such events in the case of EB3 tracks (Fig. 5 E). The protrusion distance following the encounter was similar for both proteins (0.84 ± 0.50 μm for APC-edge encounters and 0.84 ± 0.62 μm for EB3-edge encounters; $P = 0.14$; $n = 367$ for APC and 168 for EB3; Mann–Whitney two-tailed test). These data show that the branched actin networks observed at the APC-positive microtubule tips by PREM are indeed able to generate local membrane protrusions at the sites where the microtubule-delivered APC contacts the cell edge.

Loss of branched actin networks from neuronal growth cones after APC knockdown

We used RNAi to determine whether APC is needed for assembly of branched actin networks in neurons. We used two lentivirus-encoded shRNAs (sh1 and sh2), which efficiently depleted the APC protein in cultured rat hippocampal neurons, as validated by Western blotting (Fig. 5 F) and immunofluorescence (Fig. S5 A). Phalloidin staining showed that APC knockdown led to a significant loss of F-actin in neurons (Fig. 5 G) and in individual growth cones at DIV6 (Fig. S5, C and D) and DIV14 (Fig. 5, H and I), whereas the total expression levels of actin remained unchanged (Fig. 5 F). In neurons transfected with control shRNA, both axonal and dendritic growth cones exhibited typical palm-like morphology, whereas APC-depleted growth cones gained an atypical elongated spear-like shape (Fig. 5 H and Fig. S5 C). These respective shapes were maintained during growth cone motility (Fig. 5 J and Video 5). Fluorescence staining of

https://doi.org/10.1083/jcb.202003091

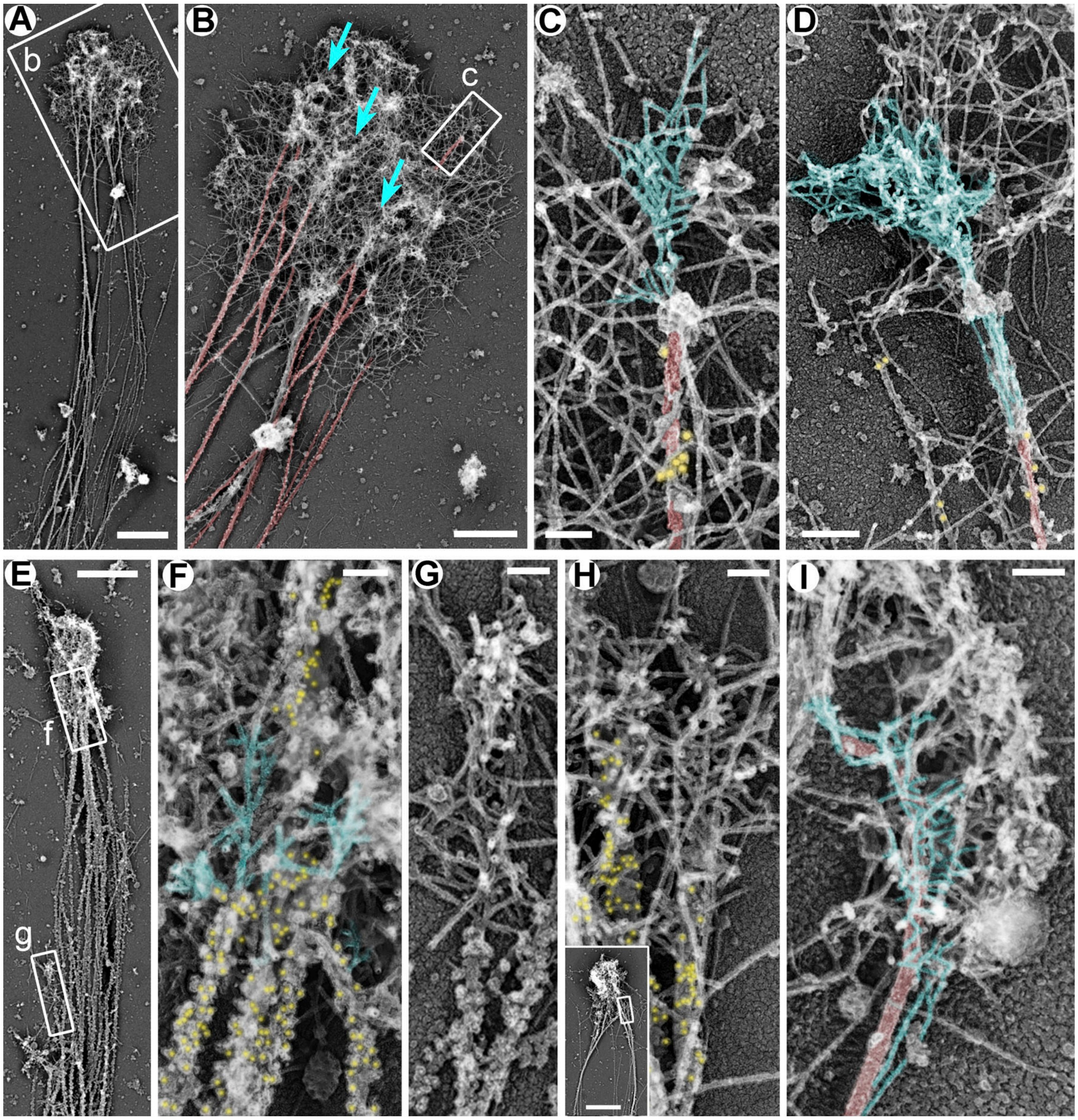

Figure 2. **Branched actin networks in growth cones of rat hippocampal neurons treated with low concentrations of actin polymerization inhibitors. (A–D)** DIV2 neurons treated for the last 24 h with 5 µM LatB and stained with DM1α antibody against α-tubulin and secondary antibody conjugated to 18-nm colloidal gold. Boxed regions in A and B are enlarged in B and C, respectively. Blue arrows in B indicate accumulations of branched actin networks that appear to emerge from microtubules. **(E–H)** DIV3 rat hippocampal neurons treated for the last 24 h with 1 µM CytoD and stained with DM1α antibody and 12-nm colloidal gold-conjugated secondary antibody. Boxed regions in E are enlarged in F and G. Inset in H shows an overview of the growth cone; the boxed region corresponds to the main panel. **(I)** DIV2 rat hippocampal neuron treated for the last 24 h with 1 µM CytoD without immunogold labeling. Color coding: blue, branched actin filaments that appear to emerge from microtubules; red, microtubules; yellow, immunogold. Scale bars, 2 µm (A and inset in H), 1 µm (B and E), 100 nm (C and F–I), and 200 nm (D).

APC-depleted DIV14 neurons with phalloidin and APC antibody revealed that the remaining growth cones in APC-depleted neurons were associated with weak accumulations of residual APC (Fig. S5 B), thus further emphasizing an important role of APC for actin assembly in neuronal growth cones.

We next used PREM to determine which subsets of actin filament arrays are impaired in APC-depleted growth cones (Fig. 6). As expected (Korobova and Svitkina, 2008), control growth cones (Fig. 6, A–D) were filled with branched actin networks abutting the growth cone edge and also contained filopodia extending beyond the leading edge. In contrast, APC-depleted growth cones (Fig. 6, E–J) were dramatically deprived of branched actin networks and mostly contained long unbranched actin filaments that extended far beyond the most distal microtubule tips in the neurites (Fig. 6, F, H, I, and L). Branched actin networks could be observed only in some APC-depleted growth cones and only as very small patches (Fig. 6, G and I–K). They were usually located at the base of the long unbranched actin extensions and often in the vicinity of the distal microtubule tips (Fig. 6 I, inset; Fig. 6 J). Quantification of the

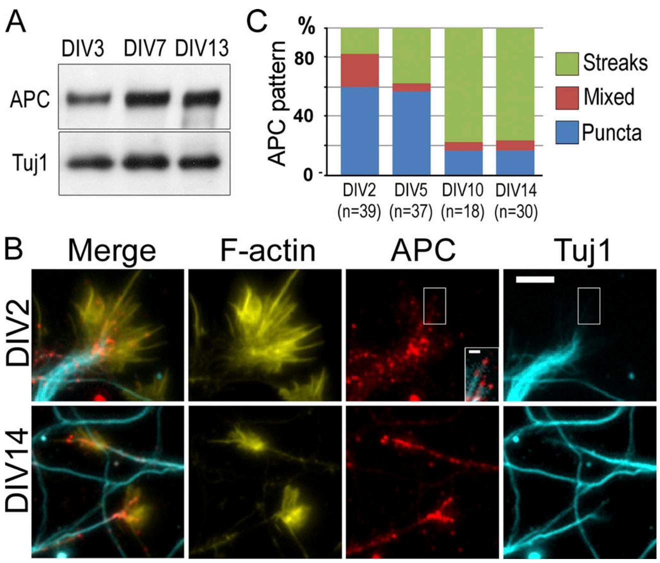

Figure 3. **Expression and localization of APC in neurons. (A)** Western blot with APC antibody of cell lysates from DIV3, 7, and 13 hippocampal neurons. Tuj1 antibody is used as loading control. **(B)** Fluorescence staining of young (DIV2) and mature (DIV14) hippocampal neurons with phalloidin (F-actin) and APC and Tuj1 antibodies. Inset in the DIV2 APC panel shows a contrast-enhanced view of the merged APC and Tuj1 signals for the boxed region. **(C)** Quantification of the APC patterns in DIV2, DIV5, DIV10, and DIV14 neurons; n corresponds to the number of scored growth cones from 17 (DIV2), 10 (DIV5), 8 (DIV10), and 9 (DIV14) cells from two independent experiments; three additional experiments were evaluated qualitatively. Scale bar, 10 µm (applies to all main panels in B) and 2 µm (inset in DIV2/APC panel).

most salient PREM features of the APC knockdown phenotype, the area of the distal cohesive regions of branched actin networks (Fig. 6 K) and the length of the longest unbranched actin extension (Fig. 6 L), in individual growth cones revealed highly significant differences between control and APC-depleted neurons. The severe loss of branched actin networks after APC depletion suggests that APC is important even for steady-state assembly of branched actin networks in growth cones, but not for assembly of unbranched actin filaments, despite an ability of APC to nucleate linear actin filaments in vitro (Breitsprecher et al., 2012; Okada et al., 2010).

Abrogation of growth cone recovery after repellent-induced collapse by APC deficiency

We next tested physiological significance of APC functions in the context of growth cone behavior. We hypothesized that APC can be particularly important to jump-start actin assembly at quiescent cell edges. For example, APC could help the growth cone to resume protrusive activity after its collapse induced by repulsive guidance cues. We mimicked such conditions by using a repulsive hormone semaphorin 3A (Sema3A; Raper, 2000) in the treatment-and-washout experiments (Fig. 7).

After Sema3A treatment, growth cones of control neurons collapsed and acquired an elongated morphology with significantly reduced F-actin contents (Fig. 7, A, C, and D). Following Sema3A washout, F-actin recovery within individual growth cones was not reliably detectable after 5 min but was nearly complete by 20 min, as the F-actin intensity at this time was not significantly different from either the original F-actin level or that at the 60-min time point, despite a trend to increase further (Fig. 7 D). It also appeared that more growth cones were present in the neuronal culture by 60 min washout (Fig. 7 C). In contrast to control neurons, growth cones of APC-depleted neurons showed neither an additional loss of F-actin after Sema3A treatment beyond that achieved by APC knockdown alone nor recovery after Sema3A washout (Fig. 7). An unexpected decrease in F-actin intensity after 5 min washout (Fig. 7 D) was reproducible in two independent experiments. It can potentially be explained by increased susceptibility of growth cones double-challenged by APC knockdown and Sema3A treatment to the mechanical impact of the washing procedure. In any case, these data show that APC is essential for recovery of growth cones after repellent-induced collapse.

Taken together, we show that APC plays key roles for the assembly of branched actin networks in association with microtubules, which is important for initiation of membrane protrusions at quiescent cell edges and for augmentation of preexisting protrusions.

Discussion

The general concept that microtubules regulate directional cell migration (Vasiliev et al., 1970) and navigation of neuronal growth cones (Tanaka and Kirschner, 1995) was established decades ago, but the underlying mechanisms are still poorly understood. Theoretically, a most straightforward scenario would be that microtubules induce actin polymerization, especially in the form of branched actin networks, which represent the main protrusive machinery in the cell that can reorient the cell leading edge in response to guidance cues (King et al., 2016; Suraneni et al., 2012; Wu et al., 2012). Recent findings support the idea that some microtubule +TIPs, such as APC (Breitsprecher et al., 2012; Okada et al., 2010) and CLIP170 (Henty-Ridilla et al., 2016), can induce assembly of unbranched actin filaments in cooperation with formins. However, a mechanism that would allow microtubules to induce assembly of Arp2/3 complex-dependent branched actin networks was previously neither supported by experimental evidence nor even seriously considered, except for the possibility that microtubules can regulate Rac1 activity, although by not yet fully defined mechanisms (van Haren et al., 2014; Waterman-Storer et al., 1999).

Our results now fill this void by showing that microtubules, with the help of APC, can locally induce assembly of branched actin networks in order to drive local protrusion or launch new protrusions after growth cone collapse. This mechanism adds a conceptually new aspect to the multifaceted actin–microtubule cross-talk in cells. It can explain not only directional cell motility (Vasiliev et al., 1970) and growth cone guidance (Tanaka et al., 1995) but also expansion of dendritic spines following the entry of microtubules (Hu et al., 2011; Jaworski et al., 2009). Although we focused on growth cones in this study, we also noticed that dendritic spines are largely absent in the APC-depleted neurons at DIV14, whereas they are normally abundant in cultured neurons of this age (Korobova and Svitkina, 2010).

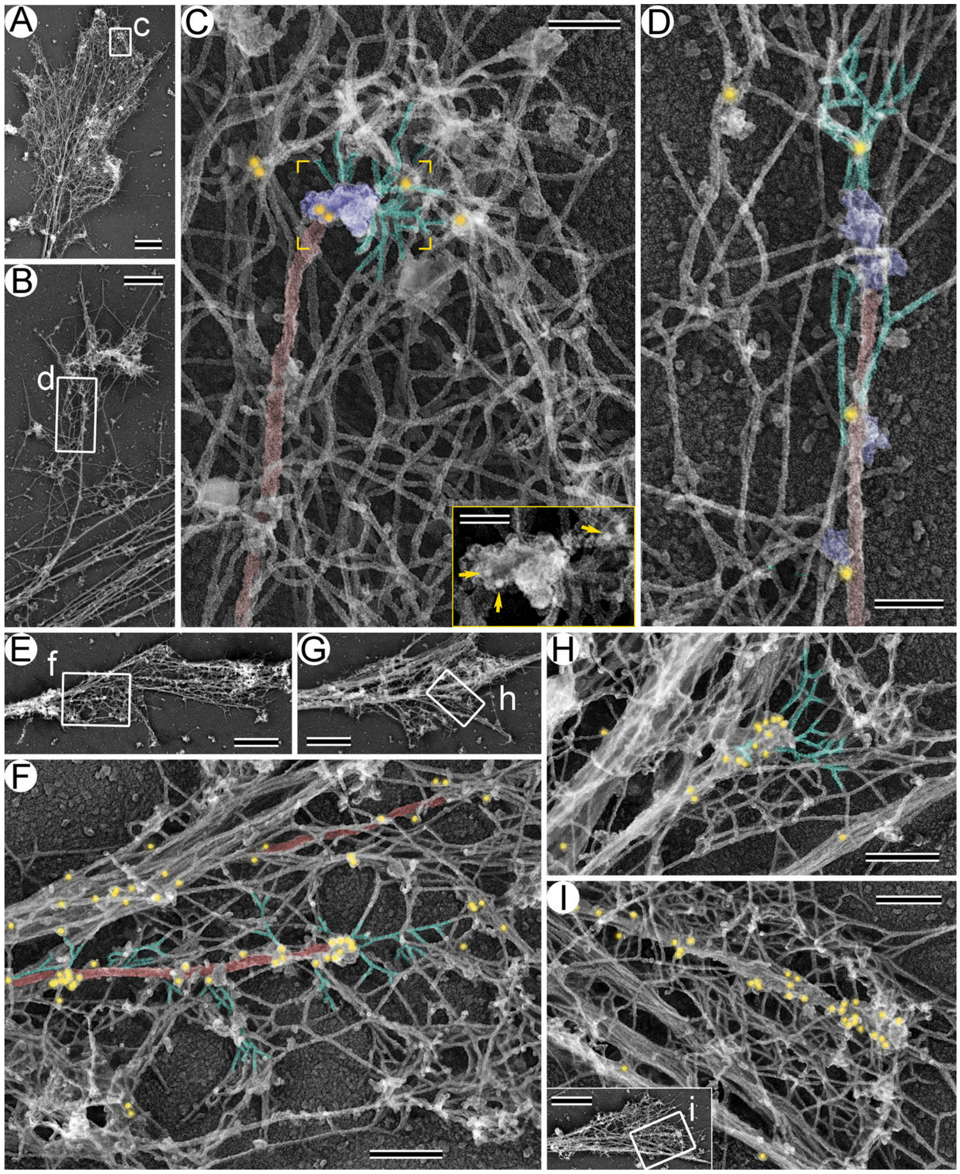

Figure 4. **Immunogold labeling of APC in neuronal growth cones. (A–D)** DIV3 neurons. **(E–I)** DIV14 neurons. A, B, E, and G and the inset in I show growth cone overviews. Boxed regions in these panels are enlarged in C, D, F, H, and I, respectively. Color coding: branched actin filaments (green), microtubules (red), putative +TIPs (purple), and 18-nm APC immunogold (yellow). Inset in C shows the yellow-framed region from the main panel without pseudocolor; yellow arrows mark APC immunogold. Scale bars, 1 µm (A, E, G, and inset in I), 500 nm (B), 200 nm (F, H, and I), 100 nm (C and D), and 50 nm (inset in C).

Our data suggest that APC is an important coordinator between microtubule dynamics and actin-based protrusion. Among numerous proteins previously proposed to mediate actin-microtubule cross-talk (Dogterom and Koenderink, 2019; Etienne-Manneville, 2013), APC appears as a best candidate. In cells, microtubule-associated APC preferentially localizes to protruding cell regions (Etienne-Manneville and Hall, 2003; Koester et al., 2007; Näthke et al., 1996), whereas APC deficiency leads to abnormal growth cone morphology and perturbed neurite outgrowth in neurons (Koester et al., 2007; Yokota et al., 2009), as well as to impaired polarized migration in nonneuronal cells (Kroboth et al., 2007; Watanabe et al., 2004). However, these phenotypes were previously explained by destabilization of microtubules in the absence of APC (Dent et al., 2011; Gordon-Weeks and Fournier, 2014), even though a link between microtubule stability and cell migration remained largely undefined. Although our results do not exclude a role of APC in regulating microtubule dynamics, we show that APC has an additional role of stimulating formation of branched actin networks in association with microtubules, which bears important novel implications for cell motility.

The mechanism by which APC induces the assembly of branched actin networks can potentially involve both of its actin-regulating activities: nucleation of unbranched actin filaments by the C terminus (Breitsprecher et al., 2012; Okada et al., 2010) and activation of the Cdc42 guanine nucleotide exchange factor Asef (Kawasaki et al., 2000; Mitin et al., 2007), and eventually of the Arp2/3 complex via Cdc42 (Gotthardt and

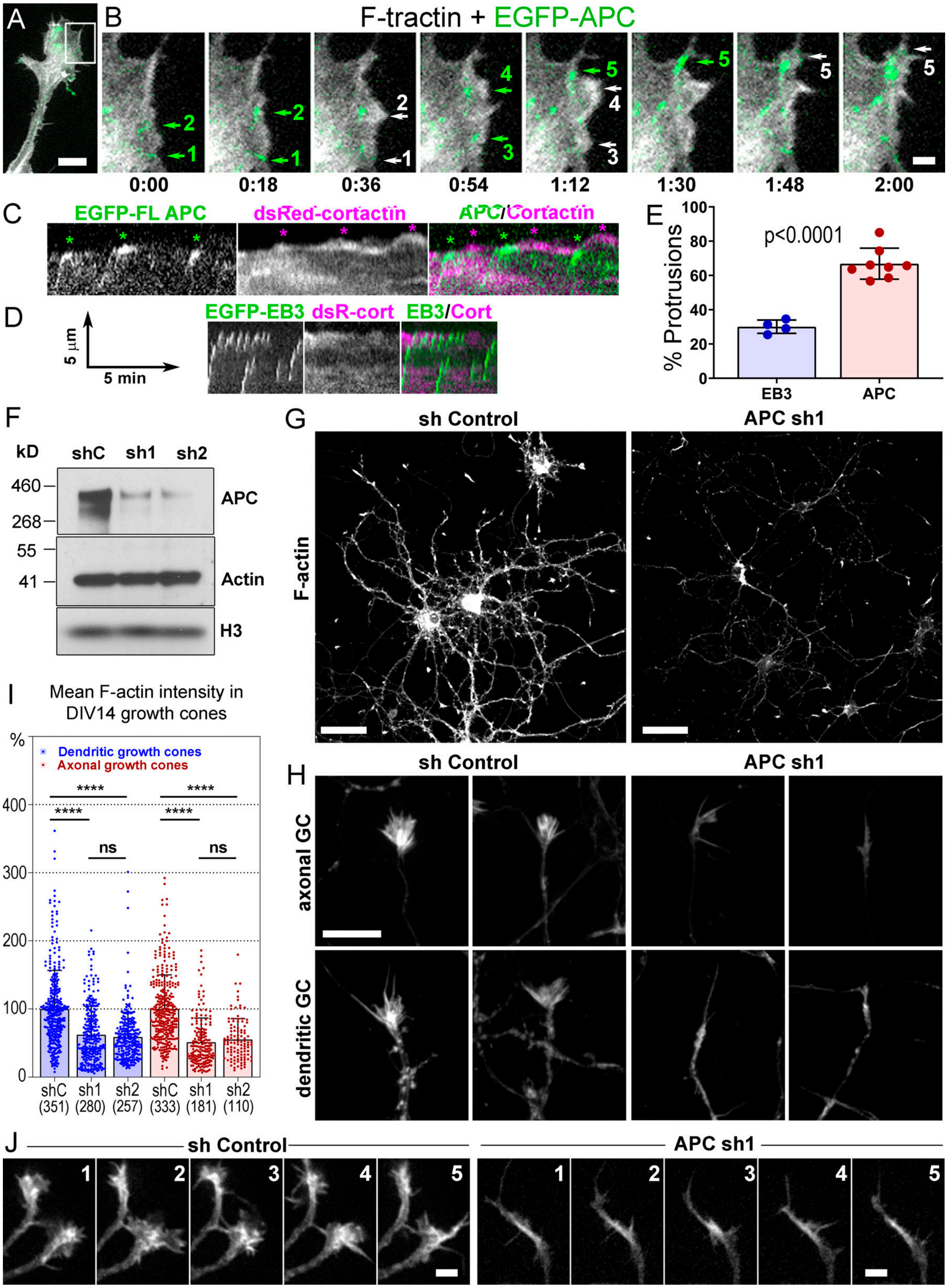

Figure 5. **Roles of APC in actin-based protrusions. (A–E)** Induction of actin-based protrusions by dynamic APC clusters in REF52 cells. **(A)** A tip of an elongated process from the cell expressing EGFP-APC (green) and mCherry-F-tractin (grayscale). **(B)** Time-lapse frames for the boxed region in A. Encounters of EGFP-APC with the cell edge (green arrows 1, 2, and 5) or preexisting lamellipodia (green arrows 3 and 4) are followed by actin-rich protrusions (white arrows with matching numbers). Green arrows 2, 4, and 5 indicate the same APC cluster sequentially hitting the cell edge. Time is shown in min:s. **(C and D)** Representative kymographs from videos of cells expressing DsRed-cortactin with either EGFP-APC (C) or EGFP-EB3 (D). **(C)** Three APC tracks hit the cell edge (green asterisks); each is followed by cortactin-rich protrusions (magenta asterisks). FL APC, full-length APC; DsC, DsRed cortactin; cort, cortactin. **(D)** EB3-edge encounters are less efficient in inducing actin-rich protrusions. Scale arrows apply to both C and D. **(E)** Percentage of EB3-edge or APC-edge encounters followed within ~30 s by actin- or cortactin-rich protrusions. Mean ± SD; *n* = 4 (EB3) and 8 (APC) independent experiments with a total number of

795 APC tracks and 545 EB3 tracks (unpaired *t* test with Welch's correction). Scale bars, 10 µm (A), 2 µm (B). **(F–J)** APC depletion in cultured rat hippocampal neurons. **(F)** Western blot of DIV14 neurons transfected at DIV1 with either control (shC), or APC-targeting (sh1 or sh2) shRNA and probed with indicated antibodies. The histone (H3) antibody is used as loading control. **(G and H)** Phalloidin staining of DIV14 neurons treated with control (sh Control) or APC-targeting (APC sh1) shRNAs. **(H)** Representative images of dendritic and axonal growth cones (GC). Scale bars, 50 µm (G) and 10 µm (H, all panels). **(I)** Average fluorescence intensity of phalloidin staining in axonal and dendritic growth cones of control and APC-depleted neurons at DIV14; mean ± SD; n (number of growth cones from 10–15 fields of view per experiment from three independent experiments for APC sh1 and two independent experiments for APC sh2, each with shControl) is shown in parenthesis for each sample; ****, P < 0.0001; ns, not significant. Kruskal–Wallis multiple comparisons test with post hoc Dunn's test. **(J)** Dynamics of mCherry-F-tractin in growth cones of control and APC-depleted neurons. Time is shown in min. Scale bars, 5 µm.

Ahmadian, 2007; Hamann et al., 2007) and N-WASP (Rohatgi et al., 1999), by its N terminus. In this appealing scenario, unbranched actin filaments nucleated by the APC's C terminus can serve as initial mother filaments to start branched actin nucleation by the Arp2/3 complex activated by the N terminus. However, we were surprised to find that unbranched actin filaments remain abundant in growth cones after APC depletion. These data suggest that APC is not necessary for nucleation of linear actin filaments in association with microtubules. In hindsight, given that binding of microtubules and actin to the C-terminal region of APC is mutually exclusive (Okada et al., 2010), this result is not totally unexpected. We propose that the main contribution of the C terminus of APC in this context is to bind microtubules, so that branched actin nucleation induced by the N terminus of APC was initiated in a spatially defined manner in association with the microtubule that delivered a cluster of APC to the plasma membrane. However, actin-nucleating activity of APC can be important in other physiological contexts. Indeed, this mechanism has been found to be involved in regulation of focal adhesion dynamics in nonneuronal cells (Juanes et al., 2017; Juanes et al., 2019).

Our results show that rather than nucleating unbranched actin filaments, APC is clearly critical for starting branched nucleation on the preexisting unbranched filaments that appear to be nucleated by other nucleators. This function of APC most likely depends on its N terminus, which has a potential to stimulate the Asef–Cdc42–N-WASP–Arp2/3 signaling pathway. This idea is consistent with the previous findings showing that the N terminus of APC has gain-of-function effects in cells (Nelson et al., 2012) and could restore normal morphology in APC knockout neurons (Chen et al., 2011). Our results that APC depletion suppresses growth cone formation appear inconsistent with previous reports showing growth cone expansions in APC-deficient neurons (Chen et al., 2011; Yokota et al., 2009). However, these authors used a conditional knockout mouse (Apc^{580S}; Shibata et al., 1997) in which Cre-mediated recombination is predicted to produce an N-terminal fragment of APC (residues 1–580). Although usually considered to be nonfunctional, this fragment actually retains the most critical residues for the interaction with Asef (Zhang et al., 2012) and thus might be able to activate Asef. Indeed, we were able to reproduce the growth cone expansion and increased branching phenotypes by transfecting Cre recombinase into cultured neurons from newborn $Apc^{580S/580S}$ mice (Fig. S5, E and F). In contrast, our shRNA-mediated strategy is not expected to produce any gain-of-function APC fragments and thus causes a real loss-of-function phenotype.

In conclusion, we reveal a new mechanism by which microtubules can regulate directional migration of neurons or nonneuronal cells. This mechanism involves stimulation of local actin-based protrusions in a microtubule-dependent manner when microtubules approach the cell leading edge. In neuronal growth cones, APC plays a central role in this process by inducing assembly of branched actin networks at microtubule tips. The N-terminal domain of APC appears to be most essential for this activity, probably by stimulating signaling that leads to Arp2/3 complex activation. This signaling is likely triggered by an APC-positive pioneer microtubule when it hits the plasma membrane, where it can encounter the downstream effectors. As a result, the growth cone or the cell leading edge would move in the direction pointed out by the pioneer microtubule. An important aspect of this model is that microtubule-associated actin assembly is not an obligatory mechanism for the formation of branched actin networks, but is employed only in special cases. For example, it can be used to achieve high precision of protrusive activity in response to external signals or be employed when a new protrusion needs to be launched at a quiescent cell edge. Both conditions are expected to frequently occur in neurons. Since precise navigation is of critical importance for neurons, it can explain the high expression levels of APC in neuronal tissues, the APC accumulation in neuronal growth cones, and the link between APC mutations and intellectual disabilities and neurological disorders (Gonzalez et al., 2015; Mohn et al., 2014; Onouchi et al., 2014).

Materials and methods

Cell culture

Dissociated rat embryo hippocampal neurons isolated as described previously (Wilcox et al., 1994) were obtained from the Neurons R Us Cell Service Core (University of Pennsylvania). In brief, hippocampi were dissected from brains of Sprague–Dawley rat embryos at embryonic day 18–20 and dissociated into individual cells by incubating in a trypsin-containing solution. The cells were then washed and plated on poly-L-lysine-coated (0.5 mg/ml) glass coverslips (for fixed cell experiments) or MatTek dishes (for live cell imaging) at concentration of 100,000 cells per 35-mm dish in 1.5 ml neurobasal medium (21103049, Thermo Fisher Scientific) with 2% B27 supplement (17504044, Thermo Fisher Scientific). Live-cell imaging was performed in an environmental chamber at 37°C in the presence of 5% CO_2. LatB (428020, Calbiochem) or CytoD (C8273, Sigma-Aldrich) was added to cultures at 12–48 h after plating from stock solutions in DMSO and cultured for an additional 24 h.

All mouse experiments were performed in compliance with the National Institutes of Health Guide for the Care and Use of Laboratory Animals and were approved by the Institutional

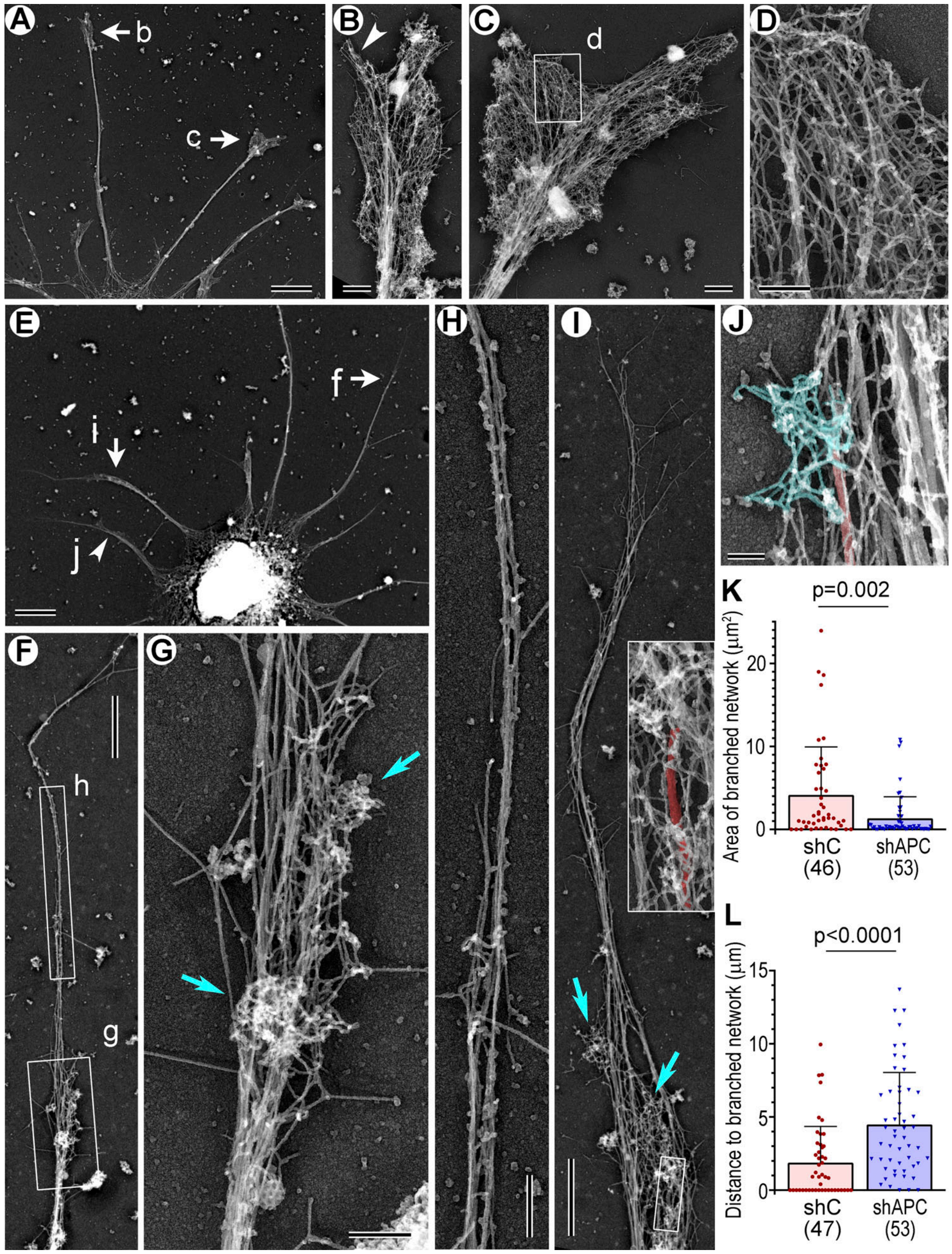

Figure 6. **PREM of control and APC-depleted rat hippocampal neurons.** Labeled arrows and boxes indicate regions enlarged in respective panels. **(A–D)** DIV6 neuron treated with control shRNA. **(A)** A part of the neuron with several dendrites. **(B and C)** Enlarged growth cones; arrowhead in B indicates a filopodium. **(D)** Enlarged view of branched actin network. **(E–J)** DIV6 neuron treated with APC sh1. **(E)** A part of the neuron with several dendrites. **(F and I)** Dendrites containing small patches of branched actin (box g in F; cyan arrows in I) and long unbranched extensions at the tips. **(G and H)** Enlarged views of branched actin patches (G, cyan arrows) and the unbranched actin extension, in which microtubules are not detectable (H). **(I)** Inset: Enlarged boxed region from the main panel. The most distal microtubule in this dendrite (red) associates with two patches of branched network, at the tip and slightly below. **(J)** A small region of the dendrite containing a microtubule (red) that terminates in a patch of branched network. **(K)** Area of most distal regions of cohesive branched network. **(L)** Lengths of the longest unbranched extensions at neurite tips. Mean ± SD; n is shown for each sample; Mann–Whitney test. One experiment was quantified; two additional experiments were evaluated qualitatively. Scale bars, 5 µm (A and E), 1 µm (F and I), 500 nm (B and C), 200 nm (D, G, and H), and 100 nm (J).

Animal Care and Use Committee at the University of Pennsylvania. Apc 580S mice (Shibata et al., 1997) were maintained on a C57/BL6N background. Genotyping was done as described previously (Shibata et al., 1997) using P3 (5′-GTTCTGTATCATGGAAAGATAGGTGGTC-3′) and P4 (5′-CACTCAAAACGCTTTTGAGGGTTGATTC-3′) primers. Mouse hippocampal neurons were isolated from brains of newborn mice and plated on poly-L-lysine–coated (1 mg/ml) coverslips in Neurobasal A medium (10888-022, Thermo Fisher Scientific) with 2% B27 supplement, 10% FBS, 1% Glutamax, and penicillin/streptomycin. After 4 h, when cells were attached, the medium was replaced with one without FBS. At DIV1, neurons were transfected with

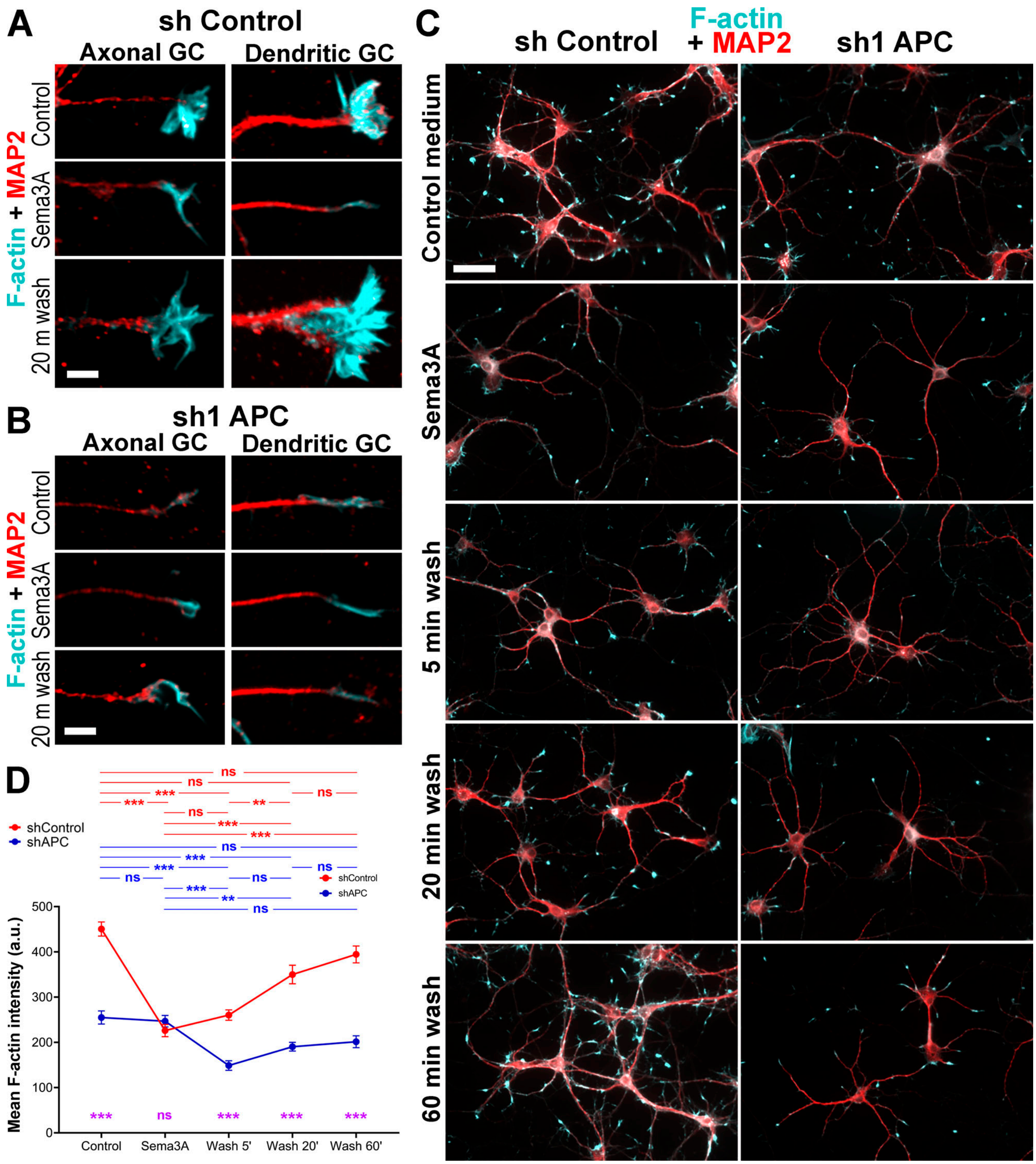

Figure 7. **APC knockdown abrogates growth cone recovery after Sema3A-induced collapse. (A–C)** Staining with phalloidin (cyan) and MAP2 antibody (red) of neurons transfected with control (A and C, left) or APC sh1 (B and C, right) shRNAs at DIV1, treated with Sema3A for 1 h at DIV7, and washed out of Sema3A for indicated periods of time. GC, growth cones. Scale bars, 5 µm (A and B) and 50 µm (C, applies to all panels). **(D)** Mean fluorescence intensity of phalloidin staining in indicated conditions. Median ± SEM; ***, P < 0.001; **, P < 0.01; ns, not significant; *n* = 51–136 growth cones from one representative experiment out of two independent experiments; Kruskal–Wallis multiple comparisons test with post hoc Dunn's test; one additional experiment was evaluated qualitatively. Purple symbols indicate significance between shControl and shAPC for respective conditions.

EGFP-tagged Cre recombinase in a lentiviral vector (Ho et al., 2006), kindly provided by T. Sudhof (Stanford University, Stanford, CA). At DIV6, hippocampal neurons from wild-type and Apc$^{580S/580s}$ mice were fixed with 4% formaldehyde in PBS and stained with Alexa Fluor 568–labeled phalloidin. Cre-expressing neurons were identified by EGFP fluorescence in the nucleus.

REF52 rat embryo fibroblasts and COS-7 green monkey kidney cells were cultured in high glucose DMEM (10569010, Thermo Fisher Scientific) supplemented with 10% FBS (F2442, Sigma-Aldrich) at 37°C and 5% CO_2. Cells were plated on glass coverslips for fixed cell experiments or on MatTek glass-bottomed dishes (MatTek Inc.) for live cell imaging. CO_2-independent phenol-red-free L15 medium (21083027, Thermo Fisher Scientific) supplemented with 10% FBS was used for live cell imaging.

Antibodies

The following rabbit polyclonal primary antibodies were used: APC-M2 against amino acids 959–1338 of APC (Wang et al., 2009), MAP2 (AB5622, Millipore), and GFP (ab6556, Abcam). The following primary mouse monoclonal antibodies were used: MAP2 (M2320, Sigma-Aldrich), pan-axonal marker SMI312 (SMI-312R, Covance), βIII tubulin (clone Tuj1, MMS-435P, Covance), α-tubulin (clone DM1α, T-6199, Sigma-Aldrich), and pan-actin (ab-5, MS-1295-P0, Thermo Fisher Scientific). Secondary antibodies and phalloidin fluorescently labeled with Alexa Fluor 488, 594, and 680 were from Invitrogen. Secondary gold-conjugated anti-rabbit (711-215-152, 18 nm; 111-205-144, 12 nm) and anti-mouse (115-215-068, 18 nm; 115-205-146, 12 nm) IgG antibodies were from Jackson ImmunoResearch Laboratories. Horseradish peroxidase–linked ECL anti-mouse (NA931V) and anti-rabbit (NA934V) IgG antibodies were from GE Healthcare.

Light microscopy

Immunofluorescence staining of neuronal cultures and non-neuronal cells was performed after fixation with 4% formaldehyde (Electron Microscopy Sciences) in PBS for 15 min followed by permeabilization with 0.3% Triton X-100 for 5 min. Confocal fluorescence microscopy was performed using a Nikon Eclipse Ti inverted microscope equipped with PlanApo 20 × 0.75 NA, CFI60 Apochromat TIRF 100 × 1.49 NA oil objective, and QuantEM 512SC digital camera (Photometrics) driven by NIS-Elements software (Nikon). Wide-field epifluorescence microscopy was performed using a Nikon Eclipse TE2000 inverted microscope equipped with Plan Apo 20 × 0.75 NA and 100 × 1.3 NA oil objectives and Cascade 512B CCD camera (Roper Scientific) driven by MetaMorph imaging software (Molecular Devices).

Electron microscopy

Sample preparation for PREM and immunogold PREM was performed as described previously (Svitkina, 2007; Svitkina, 2009) with minor modifications. In brief, detergent-extracted samples were sequentially fixed with 2% glutaraldehyde in 0.1 M Na-cacodylate buffer, pH 7.3, 0.1% tannic acid, and 0.2% uranyl acetate; critical point dried; coated with platinum and carbon; and transferred onto electron microscopic grids for observation. Detergent extraction was done with 0.5% Triton X-100 in 100 mM Pipes-KOH, pH 6.9, 1 mM $MgCl_2$, and 1 mM EGTA (PEM buffer) containing 2% polyethelene glycol (molecular weight, 35,000), 4 µM phalloidin, and 10 µM taxol for 3 min at room temperature.

For APC immunogold PREM, primary antibody in PEM buffer containing 4 µM unlabeled phalloidin and 10 µM taxol was added for 30 min either to extracted unfixed cells or to cells extracted with the same extraction solution supplemented with 0.5% formaldehyde. Samples were rinsed twice in PEM, incubated in the third change of PEM for 15 min, and fixed with 0.2% glutaraldehyde in 0.1 M cacodylate buffer for 20 min. Samples were quenched with 2 mg/ml $NaBH_4$ in PBS, incubated overnight with secondary gold-conjugated antibodies, fixed with 2% glutaraldehyde, and processed for PREM, as described above. Samples were analyzed using a JEM 1011 transmission electron microscope (JEOL) operated at 100 kV. Images were captured with an ORIUS 832.10W CCD camera (Gatan) and are presented in inverted contrast. Gold particles in PREM samples were identified at 200,000× magnification after contrast enhancement to distinguish them from other bright objects. Color labeling and image overlays were performed using Adobe Photoshop (Adobe Systems), as described previously (Shutova et al., 2012). For color segmentation, microtubules were identified by their unique thickness of ∼25 nm; branched actin networks were recognized by a combination of some or all of the following characteristics: the presence of frequent Y-shaped configurations, short filament lengths, a wide range of filament orientations, and abundance of actin filament ends within a local area of actin network.

Western blotting

Rat hippocampal neurons grown on plastic dishes coated with 0.5 mg/ml poly-L-lysine were lysed in a buffer containing 20 mM Hepes (pH 6.9), 150 mM KCl, 2 mM $MgCl_2$, 1 mM DTT, and 0.5% Triton X-100 or 30 mM Tris-HCl, pH 7.5, 150 mM NaCl, and 1% CHAPS. After clarification of lysates by centrifugation at 13,000 *g* for 10 min at 4°C, the protein concentration in supernatants was determined using Protein Assay (500-0006, BIO-RAD). Protein samples were mixed with the NuPAGE sample buffer (NP0007, Invitrogen) supplemented with 200 mM DTT and 10% glycerol and heated at 75°C for 10 min. About 20 µg (for cell lysates) of total protein was loaded onto 3–8% NuPAGE Tris-acetate 1.0 gradient gels (EA0375, Invitrogen), resolved by SDS-PAGE, and transferred to 0.45 µm nitrocellulose membrane in NuPAGE Transfer Buffer for 2 h at 20 V using the XCell SureLock Mini-Cell Electrophoresis and Western Blotting System (Invitrogen). The membrane was blocked with 5% milk in TBS (170-6435, BIO-RAD) for 1 h, incubated overnight with primary antibodies in 0.5% TBS/Tween 20 (P7949, Sigma-Aldrich) at 4°C for 2 h, washed in TBS/Tween 20, incubated with secondary antibodies (1/20,000 dilution) for 40 min, and developed with ECL Western Blotting Detection Reagent (RPN2232, GE Healthcare).

shRNA and expression constructs and transfection

The following shRNA sequences were used to target APC: 5′-ACGAGCACAGCGAAGAATAG-3′ (sh#1; Mills et al., 2016) and 5′-GCACACTGCACTGAGAATA-3′ (sh#2; Demir et al., 2013). The luciferase-targeting sequence 5′-GCCATTCTATCCTCTAGAG-3′ (shC) was used as nontargeting control. Oligos for shRNA construction were obtained from Integrated DNA Technologies, annealed, and cloned into HpaI and XhoI restriction enzyme sites of the lentiviral pLL-Cerulean 5.0 vector (kindly provided

https://doi.org/10.1083/jcb.202003091

by A. Efimov, Fox Chase Cancer Center, Philadelphia, PA; Smalley-Freed et al., 2010). For producing lentiviral particles, expression plasmids containing shRNA sequences were co-transfected together with helper plasmids MD2G and Pax2 into HEK-293T cells using FuGENE6 (E2691, Promega). Virus was harvested on the third day after transfection, filtered through 0.45 µm filter, and applied to hippocampal neurons at DIV1 together with 5 µg/ml protamine sulfate (P4020, Sigma). Culture medium was replaced after 6–8 h of incubation with the virus. Neurons were cultured for additional five or more days before analysis.

The following expression constructs were used: YFP-APC was a gift from E.M. Wenzel (The Norwegian Radium Hospital, Oslo, Norway) and J. Behrens (University of Erlangen-Nürnberg, Erlangen, Germany; Schneikert et al., 2013), cortactin-dsRed (mouse cortactin cloned into EcoR1-Sal1 sites of pDsRed2-N1 vector) was a gift from S. Kojima and G.G. Borisy (Northwestern University Feinberg School of Medicine, Chicago, IL), cortactin-pmCherryC1 (Addgene plasmid 27676) was a gift from C. Merrifield (Medical Research Council Laboratory of Molecular Biology, Cambridge, UK; Taylor et al., 2011), pLL-mCherry and pLL-EGFP vectors (Smalley-Freed et al., 2010) and pLL-EGFP-EB3 (human) construct were gifts from A. Efimov (Fox Chase Cancer Center, Philadelphia, PA). Full-length pLL-EGFP-APC was generated by PCR from the YFP-APC template and cloned into pLL-EGFP-5.0 vector. The primers were 5′-TTCGTG ACCGCGGCCAGATCTG-3′ (forward with SacII restriction site) and 5′-CAAGGGATCCACAGATGTCACAAGGTAAGACCC-3′ (reverse with BamHI restriction site). The PCR product was treated with DpnI enzyme and transformed into DH5α cells.

F-tractin–tdTomato (amino acids 9–40 from inositol-1,4,5-trisphosphate-3-kinase A fused to tdTomato; Johnson and Schell, 2009) was a gift of M. Schell (Uniformed Services University, Bethesda, MD). To generate F-tractin–mCherry and F-tractin–EGFP in lentiviral expression vectors, F-tractin prototype (amino acids 9–52) was amplified from the F-tractin–pEGFP construct using the 5′-GCTCGAATTCATGGGCATGGCG-3′ and 5′-CGGTGGATCCGA CCCTGC-3′ primers, digested with EcoRI and BamHI, and recloned into pLL-mCherry and pLL-EGFP vectors, respectively. Similarly, LifeAct (Riedl et al., 2008) was recloned from LifeAct-EGFP (gift from D. Vignjevic, Institute Curie, Paris, France) into pLL-mCherry vector after amplification using the 5′-CTTCGAATTCATGGGTGT CGCA-3′ and 5′-CGGTGGATCCCCTTCTTCC-3′ primers and digestion with EcoRI and BamHI. For transfection, subconfluent cells cultured for 15–24 h were trypsinized, collected by centrifugation at 1,200 rpm for 5 min, and electroporated using the Neon TM transfection system (MPK5000, Invitrogen) with the following parameters: voltage, 1,300 V; width, 10 ms; pulses, 3 (for COS7 cells); and voltage, 1,350 V; width, 30 ms; and pulse, 1 (for REF52 cells).

Sema3A treatment and washout

Sema3A plasmid (gift from J. Raper, University of Pennsylvania, Philadelphia, PA) was transfected into HEK-293T cells using Fugene6 transfection reagent. Medium from transfected and nontransfected (control) cell cultures was collected after 48 h of expression, filtered through a 0.45 µm syringe filter, aliquoted, and stored at −80°C. Expression efficiency was tested by Western blotting before use. The optimal dilution of Sema3A-containing medium that induced maximal reduction of F-actin staining at the lowest concentration was determined in preliminary experiments. For subsequent experiments, DIV7 neurons transfected at DIV1 with control or APC-targeting shRNAs were treated for 1 h with either control or Sema3A-containing medium. To induce recovery, Sema3A was washed out with warm neurobasal medium with B27 supplement. After different time periods of recovery, samples were fixed with 4% PFA in PBS, permeabilzed with 0.3% Triton X-100 for 5 min, and stained with phalloidin and MAP2 antibody for fluorescence microscopy.

Image analysis and statistics

Image analyses and measurements were done using Fiji (ImageJ, National Institutes of Health) or Adobe Photoshop software. Statistical analyses were performed using GraphPad Prism version 8.1.1 for Windows (GraphPad Software).

Quantification of the percentage of different actin filament arrays associated with microtubule tips in growth cones was performed using PREM images of DIV2 neurons stained with mouse DM1α tubulin antibody and 18-nm gold-conjugated anti-mouse antibody. Only clearly distinguishable microtubule tips were included in the analysis. Microtubules were categorized as the following. They were considered to be associated with (a) “branched filaments” if any actin filament physically associated with the microtubule exhibits side branch(es) along its length; (b) “branched patch” if the microtubule terminated in a local enrichment of branched actin filaments, but high network density did not allow visualization of the physical interaction of individual actin filaments with the microtubule; (c) “linear filaments” if actin filaments physically associated with the microtubules, but did not exhibit branches; (d) “filopodial bundles” if microtubules touched and were approximately aligned with bundles of long parallel actin filaments regardless of whether these bundles extended beyond the leading edge of the growth cones or not; and (e) “complex network” if microtubules were entangled with random actin filaments without obvious physical association with any of them. “Naked” microtubule tips not interacting with any actin filaments were not included into quantification.

The APC pattern in growth cones was categorized as “streaks” if immunofluorescence intensity was predominantly concentrated in elongated features with at least a 2:1 aspect ratio, as “puncta” if it represented a collection of nearly round dots, and as “mixed” if both types of clusters were present in growth cones.

Quantification of actin cytoskeleton architecture at neurite tips was performed using PREM images of DIV6 hippocampal neurons treated with control or APC-targeting shRNA starting from DIV1. Every neurite tip without technical defects or extensive overlap with other structures was included in the analysis. For determination of the area of branched actin network at the neurite tip, only the most distal cohesive region occupied by a branched network was measured excluding the filopodial regions that extended beyond the network. The distance from the extreme neurite tip to the most distal branched network was measured along the set of distal unbranched actin filaments. In control neurons, this parameter usually corresponded to the length of the longest filopodium extending beyond the branched network. If there were no branched actin networks at the neurite tip of APC-knockdown neurons, the length of the set of linear filaments was measured up to the most distal microtubule tip. Large, apparently pausing, growth cones observed in control cultures were excluded from the analysis.

Quantification of fluorescence intensities of phalloidin (F-actin marker) and APC immunofluorescence staining in growth cones was performed using Fiji software after background subtraction and thresholding of individual growth cones based on phalloidin staining. For quantifications shown in Fig. 2, neurons were imaged by epifluorescence microscopy at 100× magnification. The same regions of interest were used to determine the growth cone area and fluorescence intensities. For Figs. 4 and 7, neurons were imaged by spinning disk confocal microscopy at 20× magnification, and confocal slices were summed up in Fiji. Dendritic and axonal growth cones were identified based on staining with MAP2 antibody (dendritic marker) and in some cases also with SMI312 antibody (axonal marker).

Quantification of protrusions induced by APC-positive microtubules was performed using time-lapse sequences of REF52 cells coexpressing full-length APC or EB3 with either F-tractin or cortactin in different colors. Kymographs were generated along a straight or segmented line drawn along the path of a moving APC or EB3 signal. Only tracks that reached the cell edge or an actin-rich zone (lamellipodium) at the cell periphery were taken into consideration. If the APC signal lingered at the edge after arrival, it is still considered, but not if there was no preceding track. No lingering of the EB3 signals was observed. Cell protrusion events were scored positive if they began simultaneously with or within 30 s after the APC or EB3 track touched the cell edge or the actin-rich zone. The protrusion distance was measured using kymographs from the position of the edge at the time when the APC or EB3 track touched the edge to the point of maximal advance before the edge position plateaued or the edge began retraction or the next bout of protrusion.

Online supplemental material

Fig. S1 shows microtubule-associated branched actin networks in COS7 cells. Fig. S2 shows localization of APC in growth cones of rat hippocampal neurons treated with actin polymerization inhibitors. Fig. S3 shows a PREM control for specificity of immunogold labeling in a growth cone. Fig. S4 shows induction of membrane protrusions upon encounters of dynamic APC clusters with the cell edge. Fig. S5 shows additional fluorescence microscopy data on down-regulation of APC in hippocampal neurons. Videos 1, 2, 3, and 4 show dynamics of fluorescently tagged APC with either F-tractin or cortactin. Video 5 shows dynamics of growth cones in control and APC-depleted neurons.

Acknowledgments

We thank Drs. E.M. Wenzel, J. Behrens, S. Kojima, G.G. Borisy, A. Efimov, and T. Sudhof for generous gifts of reagents and Dr. M.S. Shutova for constructing the control luciferase-targeting shRNA.

This work supported by National Institutes of Health grants R01 GM 095977 to T.M. Svitkina, R01 CA 168654 to C.J. Lengner, R50 CA 221841 to N. Li, and R01 CA 109220 to K.L. Neufeld.

The authors declare no competing financial interests.

Author contributions: N. Efimova, C. Yang, and J.X. Chia performed experiments and analyzed data; K.L. Neufeld provided reagents; C.J. Lengner supervised mouse work; N. Li performed mouse breeding and genotyping; T.M. Svitkina oversaw research and wrote the manuscript.

Submitted: 16 March 2020
Revised: 26 May 2020
Accepted: 28 May 2020

References

Alves-Silva, J., N. Sánchez-Soriano, R. Beaven, M. Klein, J. Parkin, T.H. Millard, H.J. Bellen, K.J. Venken, C. Ballestrem, R.A. Kammerer, et al. 2012. Spectraplakins promote microtubule-mediated axonal growth by functioning as structural microtubule-associated proteins and EB1-dependent +TIPs (tip interacting proteins). *J. Neurosci.* 32:9143–9158. https://doi.org/10.1523/JNEUROSCI.0416-12.2012

Bearce, E.A., B. Erdogan, and L.A. Lowery. 2015. TIPsy tour guides: how microtubule plus-end tracking proteins (+TIPs) facilitate axon guidance. *Front. Cell. Neurosci.* 9:241. https://doi.org/10.3389/fncel.2015.00241

Bhat, R.V., J.M. Baraban, R.C. Johnson, B.A. Eipper, and R.E. Mains. 1994. High levels of expression of the tumor suppressor gene APC during development of the rat central nervous system. *J. Neurosci.* 14:3059–3071. https://doi.org/10.1523/JNEUROSCI.14-05-03059.1994

Blanquie, O., and F. Bradke. 2018. Cytoskeleton dynamics in axon regeneration. *Curr. Opin. Neurobiol.* 51:60–69. https://doi.org/10.1016/j.conb.2018.02.024

Breitsprecher, D., R. Jaiswal, J.P. Bombardier, C.J. Gould, J. Gelles, and B.L. Goode. 2012. Rocket launcher mechanism of collaborative actin assembly defined by single-molecule imaging. *Science.* 336:1164–1168. https://doi.org/10.1126/science.1218062

Buck, K.B., and J.Q. Zheng. 2002. Growth cone turning induced by direct local modification of microtubule dynamics. *J. Neurosci.* 22:9358–9367. https://doi.org/10.1523/JNEUROSCI.22-21-09358.2002

Burnette, D.T., A.W. Schaefer, L. Ji, G. Danuser, and P. Forscher. 2007. Filopodial actin bundles are not necessary for microtubule advance into the peripheral domain of Aplysia neuronal growth cones. *Nat. Cell Biol.* 9: 1360–1369. https://doi.org/10.1038/ncb1655

Cammarata, G.M., E.A. Bearce, and L.A. Lowery. 2016. Cytoskeletal social networking in the growth cone: How +TIPs mediate microtubule-actin cross-linking to drive axon outgrowth and guidance. *Cytoskeleton (Hoboken).* 73:461–476. https://doi.org/10.1002/cm.21272

Chen, Y., X. Tian, W.Y. Kim, and W.D. Snider. 2011. Adenomatous polyposis coli regulates axon arborization and cytoskeleton organization via its N-terminus. *PLoS One.* 6. e24335. https://doi.org/10.1371/journal.pone.0024335

Chia, J.X., N. Efimova, and T.M. Svitkina. 2016. Neurite outgrowth is driven by actin polymerization even in the presence of actin polymerization inhibitors. *Mol. Biol. Cell.* 27:3695–3704. https://doi.org/10.1091/mbc.e16-04-0253

Demir, K., N. Kirsch, C.A. Beretta, G. Erdmann, D. Ingelfinger, E. Moro, F. Argenton, M. Carl, C. Niehrs, and M. Boutros. 2013. RAB8B is required for activity and caveolar endocytosis of LRP6. *Cell Rep.* 4:1224–1234. https://doi.org/10.1016/j.celrep.2013.08.008

Dent, E.W., and K. Kalil. 2001. Axon branching requires interactions between dynamic microtubules and actin filaments. *J. Neurosci.* 21:9757–9769. https://doi.org/10.1523/JNEUROSCI.21-24-09757.2001

Dent, E.W., F. Tang, and K. Kalil. 2003. Axon guidance by growth cones and branches: common cytoskeletal and signaling mechanisms. *Neuroscientist.* 9:343–353. https://doi.org/10.1177/1073858403252683

Dent, E.W., A.V. Kwiatkowski, L.M. Mebane, U. Philippar, M. Barzik, D.A. Rubinson, S. Gupton, J.E. Van Veen, C. Furman, J. Zhang, et al. 2007. Filopodia are required for cortical neurite initiation. *Nat. Cell Biol.* 9: 1347–1359. https://doi.org/10.1038/ncb1654

Dent, E.W., S.L. Gupton, and F.B. Gertler. 2011. The growth cone cytoskeleton in axon outgrowth and guidance. *Cold Spring Harb. Perspect. Biol.* 3. a001800. https://doi.org/10.1101/cshperspect.a001800

Dogterom, M., and G.H. Koenderink. 2019. Actin-microtubule crosstalk in cell biology. *Nat. Rev. Mol. Cell Biol.* 20:38–54. https://doi.org/10.1038/s41580-018-0067-1

Eira, J., C.S. Silva, M.M. Sousa, and M.A. Liz. 2016. The cytoskeleton as a novel therapeutic target for old neurodegenerative disorders. *Prog. Neurobiol.* 141:61–82. https://doi.org/10.1016/j.pneurobio.2016.04.007

Engle, E.C.. 2010. Human genetic disorders of axon guidance. *Cold Spring Harb. Perspect. Biol.* 2. a001784. https://doi.org/10.1101/cshperspect.a001784

Etienne-Manneville, S.. 2013. Microtubules in cell migration. *Annu. Rev. Cell Dev. Biol.* 29:471–499. https://doi.org/10.1146/annurev-cellbio-101011-155711

Etienne-Manneville, S., and A. Hall. 2003. Cdc42 regulates GSK-3beta and adenomatous polyposis coli to control cell polarity. *Nature*. 421:753–756. https://doi.org/10.1038/nature01423

Geraldo, S., U.K. Khanzada, M. Parsons, J.K. Chilton, and P.R. Gordon-Weeks. 2008. Targeting of the F-actin-binding protein drebrin by the microtubule plus-tip protein EB3 is required for neuritogenesis. *Nat. Cell Biol.* 10:1181–1189. https://doi.org/10.1038/ncb1778

Gonzalez, L., J. Alvarez, E. Weinstein, and P. Korenis. 2015. Familial adenomatous polyposis in an adolescent with coexisting schizophrenia: treatment strategies and implications. *Mol. Genet. Genomic Med.* 3: 391–395. https://doi.org/10.1002/mgg3.114

Gordon-Weeks, P.R., and A.E. Fournier. 2014. Neuronal cytoskeleton in synaptic plasticity and regeneration. *J. Neurochem.* 129:206–212. https://doi.org/10.1111/jnc.12502

Gotthardt, K., and M.R. Ahmadian. 2007. Asef is a Cdc42-specific guanine nucleotide exchange factor. *Biol. Chem.* 388:67–71. https://doi.org/10.1515/BC.2007.008

Hamann, M.J., C.M. Lubking, D.N. Luchini, and D.D. Billadeau. 2007. Asef2 functions as a Cdc42 exchange factor and is stimulated by the release of an autoinhibitory module from a concealed C-terminal activation element. *Mol. Cell. Biol.* 27:1380–1393. https://doi.org/10.1128/MCB.01608-06

Henty-Ridilla, J.L., A. Rankova, J.A. Eskin, K. Kenny, and B.L. Goode. 2016. Accelerated actin filament polymerization from microtubule plus ends. *Science*. 352:1004–1009. https://doi.org/10.1126/science.aaf1709

Ho, A., W. Morishita, D. Atasoy, X. Liu, K. Tabuchi, R.E. Hammer, R.C. Malenka, and T.C. Südhof. 2006. Genetic analysis of Mint/X11 proteins: essential presynaptic functions of a neuronal adaptor protein family. *J. Neurosci.* 26:13089–13101. https://doi.org/10.1523/JNEUROSCI.2855-06.2006

Hu, X., L. Ballo, L. Pietila, C. Viesselmann, J. Ballweg, D. Lumbard, M. Stevenson, E. Merriam, and E.W. Dent. 2011. BDNF-induced increase of PSD-95 in dendritic spines requires dynamic microtubule invasions. *J. Neurosci.* 31:15597–15603. https://doi.org/10.1523/JNEUROSCI.2445-11.2011

Hu, J., X. Bai, J.R. Bowen, L. Dolat, F. Korobova, W. Yu, P.W. Baas, T. Svitkina, G. Gallo, and E.T. Spiliotis. 2012. Septin-driven coordination of actin and microtubule remodeling regulates the collateral branching of axons. *Curr. Biol.* 22:1109–1115. https://doi.org/10.1016/j.cub.2012.04.019

Jaworski, J., L.C. Kapitein, S.M. Gouveia, B.R. Dortland, P.S. Wulf, I. Grigoriev, P. Camera, S.A. Spangler, P. Di Stefano, J. Demmers, et al. 2009. Dynamic microtubules regulate dendritic spine morphology and synaptic plasticity. *Neuron*. 61:85–100. https://doi.org/10.1016/j.neuron.2008.11.013

Jiang, K., and A. Akhmanova. 2011. Microtubule tip-interacting proteins: a view from both ends. *Curr. Opin. Cell Biol.* 23:94–101. https://doi.org/10.1016/j.ceb.2010.08.008

Johnson, H.W., and M.J. Schell. 2009. Neuronal IP3 3-kinase is an F-actin-bundling protein: role in dendritic targeting and regulation of spine morphology. *Mol. Biol. Cell.* 20:5166–5180. https://doi.org/10.1091/mbc.e09-01-0083

Juanes, M.A., H. Bouguenina, J.A. Eskin, R. Jaiswal, A. Badache, and B.L. Goode. 2017. Adenomatous polyposis coli nucleates actin assembly to drive cell migration and microtubule-induced focal adhesion turnover. *J. Cell Biol.* 216:2859–2875. https://doi.org/10.1083/jcb.201702007

Juanes, M.A., D. Isnardon, A. Badache, S. Brasselet, M. Mavrakis, and B.L. Goode. 2019. The role of APC-mediated actin assembly in microtubule capture and focal adhesion turnover. *J. Cell Biol.* 218:3415–3435. https://doi.org/10.1083/jcb.201904165

Kaverina, I., O. Krylyshkina, and J.V. Small. 1999. Microtubule targeting of substrate contacts promotes their relaxation and dissociation. *J. Cell Biol.* 146:1033–1044. https://doi.org/10.1083/jcb.146.5.1033

Kawasaki, Y., T. Senda, T. Ishidate, R. Koyama, T. Morishita, Y. Iwayama, O. Higuchi, and T. Akiyama. 2000. Asef, a link between the tumor suppressor APC and G-protein signaling. *Science*. 289:1194–1197. https://doi.org/10.1126/science.289.5482.1194

King, S.J., S.B. Asokan, E.M. Haynes, S.P. Zimmerman, J.D. Rotty, J.G. Alb, Jr., A. Tagliatela, D.R. Blake, I.P. Lebedeva, D. Marston, et al. 2016. Lamellipodia are crucial for haptotactic sensing and response. *J. Cell Sci.* 129: 2329–2342. https://doi.org/10.1242/jcs.184507

Kita, K., T. Wittmann, I.S. Näthke, and C.M. Waterman-Storer. 2006. Adenomatous polyposis coli on microtubule plus ends in cell extensions can promote microtubule net growth with or without EB1. *Mol. Biol. Cell.* 17: 2331–2345. https://doi.org/10.1091/mbc.e05-06-0498

Koester, M.P., O. Müller, and G.E. Pollerberg. 2007. Adenomatous polyposis coli is differentially distributed in growth cones and modulates their steering. *J. Neurosci.* 27:12590–12600. https://doi.org/10.1523/JNEUROSCI.2250-07.2007

Korobova, F., and T. Svitkina. 2008. Arp2/3 complex is important for filopodia formation, growth cone motility, and neuritogenesis in neuronal cells. *Mol. Biol. Cell.* 19:1561–1574. https://doi.org/10.1091/mbc.e07-09-0964

Korobova, F., and T. Svitkina. 2010. Molecular architecture of synaptic actin cytoskeleton in hippocampal neurons reveals a mechanism of dendritic spine morphogenesis. *Mol. Biol. Cell.* 21:165–176. https://doi.org/10.1091/mbc.e09-07-0596

Krendel, M., F.T. Zenke, and G.M. Bokoch. 2002. Nucleotide exchange factor GEF-H1 mediates cross-talk between microtubules and the actin cytoskeleton. *Nat. Cell Biol.* 4:294–301. https://doi.org/10.1038/ncb773

Kroboth, K., I.P. Newton, K. Kita, D. Dikovskaya, J. Zumbrunn, C.M. Waterman-Storer, and I.S. Näthke. 2007. Lack of adenomatous polyposis coli protein correlates with a decrease in cell migration and overall changes in microtubule stability. *Mol. Biol. Cell.* 18:910–918. https://doi.org/10.1091/mbc.e06-03-0179

Machesky, L.M., R.D. Mullins, H.N. Higgs, D.A. Kaiser, L. Blanchoin, R.C. May, M.E. Hall, and T.D. Pollard. 1999. Scar, a WASp-related protein, activates nucleation of actin filaments by the Arp2/3 complex. *Proc. Natl. Acad. Sci. USA.* 96:3739–3744. https://doi.org/10.1073/pnas.96.7.3739

Mills, K.M., M.G. Brocardo, and B.R. Henderson. 2016. APC binds the Miro/Milton motor complex to stimulate transport of mitochondria to the plasma membrane. *Mol. Biol. Cell.* 27:466–482. https://doi.org/10.1091/mbc.e15-09-0632

Mimori-Kiyosue, Y., N. Shiina, and S. Tsukita. 2000. Adenomatous polyposis coli (APC) protein moves along microtubules and concentrates at their growing ends in epithelial cells. *J. Cell Biol.* 148:505–518. https://doi.org/10.1083/jcb.148.3.505

Mitin, N., L. Betts, M.E. Yohe, C.J. Der, J. Sondek, and K.L. Rossman. 2007. Release of autoinhibition of ASEF by APC leads to CDC42 activation and tumor suppression. *Nat. Struct. Mol. Biol.* 14:814–823. https://doi.org/10.1038/nsmb1290

Mohn, J.L., J. Alexander, A. Pirone, C.D. Palka, S.Y. Lee, L. Mebane, P.G. Haydon, and M.H. Jacob. 2014. Adenomatous polyposis coli protein deletion leads to cognitive and autism-like disabilities. *Mol. Psychiatry.* 19:1133–1142. https://doi.org/10.1038/mp.2014.61

Moseley, J.B., F. Bartolini, K. Okada, Y. Wen, G.G. Gundersen, and B.L. Goode. 2007. Regulated binding of adenomatous polyposis coli protein to actin. *J. Biol. Chem.* 282:12661–12668. https://doi.org/10.1074/jbc.M610615200

Mullins, R.D., J.A. Heuser, and T.D. Pollard. 1998. The interaction of Arp2/3 complex with actin: nucleation, high affinity pointed end capping, and formation of branching networks of filaments. *Proc. Natl. Acad. Sci. USA.* 95:6181–6186. https://doi.org/10.1073/pnas.95.11.6181

Muñoz-Lasso, D.C., C. Romá-Mateo, F.V. Pallardó, and P. Gonzalez-Cabo. 2020. Much more than a scaffold: Cytoskeletal proteins in neurological disorders. *Cells*. 9:358. https://doi.org/10.3390/cells9020358

Myers, K.A., I. Tint, C.V. Nadar, Y. He, M.M. Black, and P.W. Baas. 2006. Antagonistic forces generated by cytoplasmic dynein and myosin-II during growth cone turning and axonal retraction. *Traffic*. 7: 1333–1351. https://doi.org/10.1111/j.1600-0854.2006.00476.x

Näthke, I.S., C.L. Adams, P. Polakis, J.H. Sellin, and W.J. Nelson. 1996. The adenomatous polyposis coli tumor suppressor protein localizes to plasma membrane sites involved in active cell migration. *J. Cell Biol.* 134: 165–179. https://doi.org/10.1083/jcb.134.1.165

Nelson, S., and I.S. Näthke. 2013. Interactions and functions of the adenomatous polyposis coli (APC) protein at a glance. *J. Cell Sci.* 126: 873–877. https://doi.org/10.1242/jcs.100479

Nelson, S.A., Z. Li, I.P. Newton, D. Fraser, R.E. Milne, D.M. Martin, D. Schiffmann, X. Yang, D. Dormann, C.J. Weijer, et al. 2012. Tumorigenic fragments of APC cause dominant defects in directional cell migration

in multiple model systems. *Dis. Model. Mech.* 5:940–947. https://doi.org/10.1242/dmm.008607
Okada, K., F. Bartolini, A.M. Deaconescu, J.B. Moseley, Z. Dogic, N. Grigorieff, G.G. Gundersen, and B.L. Goode. 2010. Adenomatous polyposis coli protein nucleates actin assembly and synergizes with the formin mDia1. *J. Cell Biol.* 189:1087–1096. https://doi.org/10.1083/jcb.201001016
Onouchi, T., K. Kobayashi, K. Sakai, A. Shimomura, R. Smits, C. Sumi-Ichinose, M. Kurosumi, K. Takao, R. Nomura, A. Iizuka-Kogo, et al. 2014. Targeted deletion of the C-terminus of the mouse adenomatous polyposis coli tumor suppressor results in neurologic phenotypes related to schizophrenia. *Mol. Brain.* 7:21. https://doi.org/10.1186/1756-6606-7-21
Pacheco, A., and G. Gallo. 2016. Actin filament-microtubule interactions in axon initiation and branching. *Brain Res. Bull.* 126:300–310. https://doi.org/10.1016/j.brainresbull.2016.07.013
Raper, J.A.. 2000. Semaphorins and their receptors in vertebrates and invertebrates. *Curr. Opin. Neurobiol.* 10:88–94. https://doi.org/10.1016/S0959-4388(99)00057-4
Riedl, J., A.H. Crevenna, K. Kessenbrock, J.H. Yu, D. Neukirchen, M. Bista, F. Bradke, D. Jenne, T.A. Holak, Z. Werb, et al. 2008. Lifeact: a versatile marker to visualize F-actin. *Nat. Methods.* 5:605–607. https://doi.org/10.1038/nmeth.1220
Rohatgi, R., L. Ma, H. Miki, M. Lopez, T. Kirchhausen, T. Takenawa, and M.W. Kirschner. 1999. The interaction between N-WASP and the Arp2/3 complex links Cdc42-dependent signals to actin assembly. *Cell.* 97:221–231. https://doi.org/10.1016/S0092-8674(00)80732-1
Schaefer, A.W., N. Kabir, and P. Forscher. 2002. Filopodia and actin arcs guide the assembly and transport of two populations of microtubules with unique dynamic parameters in neuronal growth cones. *J. Cell Biol.* 158:139–152. https://doi.org/10.1083/jcb.200203038
Schneikert, J., S.H. Vijaya Chandra, J.G. Ruppert, S. Ray, E.M. Wenzel, and J. Behrens. 2013. Functional comparison of human adenomatous polyposis coli (APC) and APC-like in targeting beta-catenin for degradation. *PLoS One.* 8. e68072. https://doi.org/10.1371/journal.pone.0068072
Shibata, H., K. Toyama, H. Shioya, M. Ito, M. Hirota, S. Hasegawa, H. Matsumoto, H. Takano, T. Akiyama, K. Toyoshima, et al. 1997. Rapid colorectal adenoma formation initiated by conditional targeting of the Apc gene. *Science.* 278:120–123. https://doi.org/10.1126/science.278.5335.120
Shutova, M., C. Yang, J.M. Vasiliev, and T. Svitkina. 2012. Functions of nonmuscle myosin II in assembly of the cellular contractile system. *PLoS One.* 7. e40814. https://doi.org/10.1371/journal.pone.0040814
Smalley-Freed, W.G., A. Efimov, P.E. Burnett, S.P. Short, M.A. Davis, D.L. Gumucio, M.K. Washington, R.J. Coffey, and A.B. Reynolds. 2010. p120-catenin is essential for maintenance of barrier function and intestinal homeostasis in mice. *J. Clin. Invest.* 120:1824–1835. https://doi.org/10.1172/JCI41414
Suraneni, P., B. Rubinstein, J.R. Unruh, M. Durnin, D. Hanein, and R. Li. 2012. The Arp2/3 complex is required for lamellipodia extension and directional fibroblast cell migration. *J. Cell Biol.* 197:239–251. https://doi.org/10.1083/jcb.201112113
Svitkina, T.. 2007. Electron microscopic analysis of the leading edge in migrating cells. *Methods Cell Biol.* 79:295–319. https://doi.org/10.1016/S0091-679X(06)79012-4
Svitkina, T.. 2009. Imaging Cytoskeleton Components by Electron Microscopy. *In Methods Mol Biol - Cytoskeleton Methods and Protocols.* Vol. Vol. 586. R.H. Gavin, editor. Humana Press, New Jersey. pp. 187–206. https://doi.org/10.1007/978-1-60761-376-3_10
Svitkina, T.M.. 2017. Platinum replica electron microscopy: Imaging the cytoskeleton globally and locally. *Int. J. Biochem. Cell Biol.* 86:37–41. https://doi.org/10.1016/j.biocel.2017.03.009
Svitkina, T.. 2018. The actin cytoskeleton and actin-based motility. *Cold Spring Harb. Perspect. Biol.* 10. a018267. https://doi.org/10.1101/cshperspect.a018267
Svitkina, T.M., and G.G. Borisy. 1999. Arp2/3 complex and actin depolymerizing factor/cofilin in dendritic organization and treadmilling of actin filament array in lamellipodia. *J. Cell Biol.* 145:1009–1026. https://doi.org/10.1083/jcb.145.5.1009
Tanaka, E., and M.W. Kirschner. 1995. The role of microtubules in growth cone turning at substrate boundaries. *J. Cell Biol.* 128:127–137. https://doi.org/10.1083/jcb.128.1.127
Tanaka, E., T. Ho, and M.W. Kirschner. 1995. The role of microtubule dynamics in growth cone motility and axonal growth. *J. Cell Biol.* 128:139–155. https://doi.org/10.1083/jcb.128.1.139
Taylor, M.J., D. Perrais, and C.J. Merrifield. 2011. A high precision survey of the molecular dynamics of mammalian clathrin-mediated endocytosis. *PLoS Biol.* 9. e1000604. https://doi.org/10.1371/journal.pbio.1000604
Tint, I., D. Jean, P.W. Baas, and M.M. Black. 2009. Doublecortin associates with microtubules preferentially in regions of the axon displaying actin-rich protrusive structures. *J. Neurosci.* 29:10995–11010. https://doi.org/10.1523/JNEUROSCI.3399-09.2009
van Haren, J., J. Boudeau, S. Schmidt, S. Basu, Z. Liu, D. Lammers, J. Demmers, J. Benhari, F. Grosveld, A. Debant, et al. 2014. Dynamic microtubules catalyze formation of navigator-TRIO complexes to regulate neurite extension. *Curr. Biol.* 24:1778–1785. https://doi.org/10.1016/j.cub.2014.06.037
Vasiliev, J.M., I.M. Gelfand, L.V. Domnina, O.Y. Ivanova, S.G. Komm, and L.V. Olshevskaja. 1970. Effect of colcemid on the locomotory behaviour of fibroblasts. *J. Embryol. Exp. Morphol.* 24:625–640.
Wang, Y., Y. Azuma, D.B. Friedman, R.J. Coffey, and K.L. Neufeld. 2009. Novel association of APC with intermediate filaments identified using a new versatile APC antibody. *BMC Cell Biol.* 10:75. https://doi.org/10.1186/1471-2121-10-75
Watanabe, T., S. Wang, J. Noritake, K. Sato, M. Fukata, M. Takefuji, M. Nakagawa, N. Izumi, T. Akiyama, and K. Kaibuchi. 2004. Interaction with IQGAP1 links APC to Rac1, Cdc42, and actin filaments during cell polarization and migration. *Dev. Cell.* 7:871–883. https://doi.org/10.1016/j.devcel.2004.10.017
Waterman-Storer, C.M., R.A. Worthylake, B.P. Liu, K. Burridge, and E.D. Salmon. 1999. Microtubule growth activates Rac1 to promote lamellipodial protrusion in fibroblasts. *Nat. Cell Biol.* 1:45–50. https://doi.org/10.1038/9018
Wilcox, K.S., J. Buchhalter, and M.A. Dichter. 1994. Properties of inhibitory and excitatory synapses between hippocampal neurons in very low density cultures. *Synapse.* 18:128–151. https://doi.org/10.1002/syn.890180206
Wu, C., S.B. Asokan, M.E. Berginski, E.M. Haynes, N.E. Sharpless, J.D. Griffith, S.M. Gomez, and J.E. Bear. 2012. Arp2/3 is critical for lamellipodia and response to extracellular matrix cues but is dispensable for chemotaxis. *Cell.* 148:973–987. https://doi.org/10.1016/j.cell.2011.12.034
Yokota, Y., W.Y. Kim, Y. Chen, X. Wang, A. Stanco, Y. Komuro, W. Snider, and E.S. Anton. 2009. The adenomatous polyposis coli protein is an essential regulator of radial glial polarity and construction of the cerebral cortex. *Neuron.* 61:42–56. https://doi.org/10.1016/j.neuron.2008.10.053
Zhang, L., and J.W. Shay. 2017. Multiple roles of APC and its therapeutic implications in colorectal cancer. *J. Natl. Cancer Inst.* 109. djw332. https://doi.org/10.1093/jnci/djw332
Zhang, Z., L. Chen, L. Gao, K. Lin, L. Zhu, Y. Lu, X. Shi, Y. Gao, J. Zhou, P. Xu, et al. 2012. Structural basis for the recognition of Asef by adenomatous polyposis coli. *Cell Res.* 22:372–386. https://doi.org/10.1038/cr.2011.119
Zhou, F.Q., C.M. Waterman-Storer, and C.S. Cohan. 2002. Focal loss of actin bundles causes microtubule redistribution and growth cone turning. *J. Cell Biol.* 157:839–849. https://doi.org/10.1083/jcb.200112014
Zumbrunn, J., K. Kinoshita, A.A. Hyman, and I.S. Näthke. 2001. Binding of the adenomatous polyposis coli protein to microtubules increases microtubule stability and is regulated by GSK3 beta phosphorylation. *Curr. Biol.* 11:44–49. https://doi.org/10.1016/S0960-9822(01)00002-1

Supplemental material

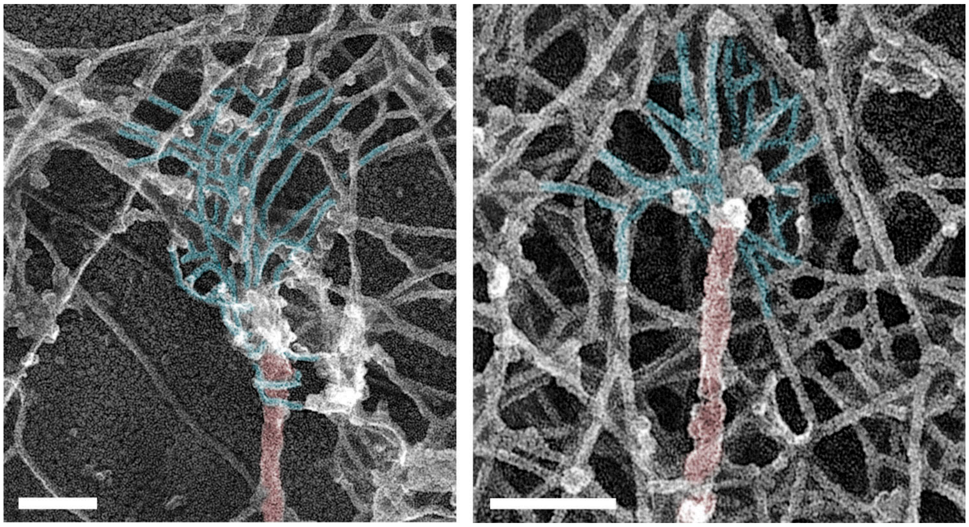

Figure S1. **Branched actin networks in COS7 cells physically linked to microtubule tips.** PREM of subcellular regions near the cell edge. Color coding indicates microtubules (red) and branched actin networks associated with microtubules (light blue). Scale bars, 100 nm.

https://doi.org/10.1083/jcb.202003091

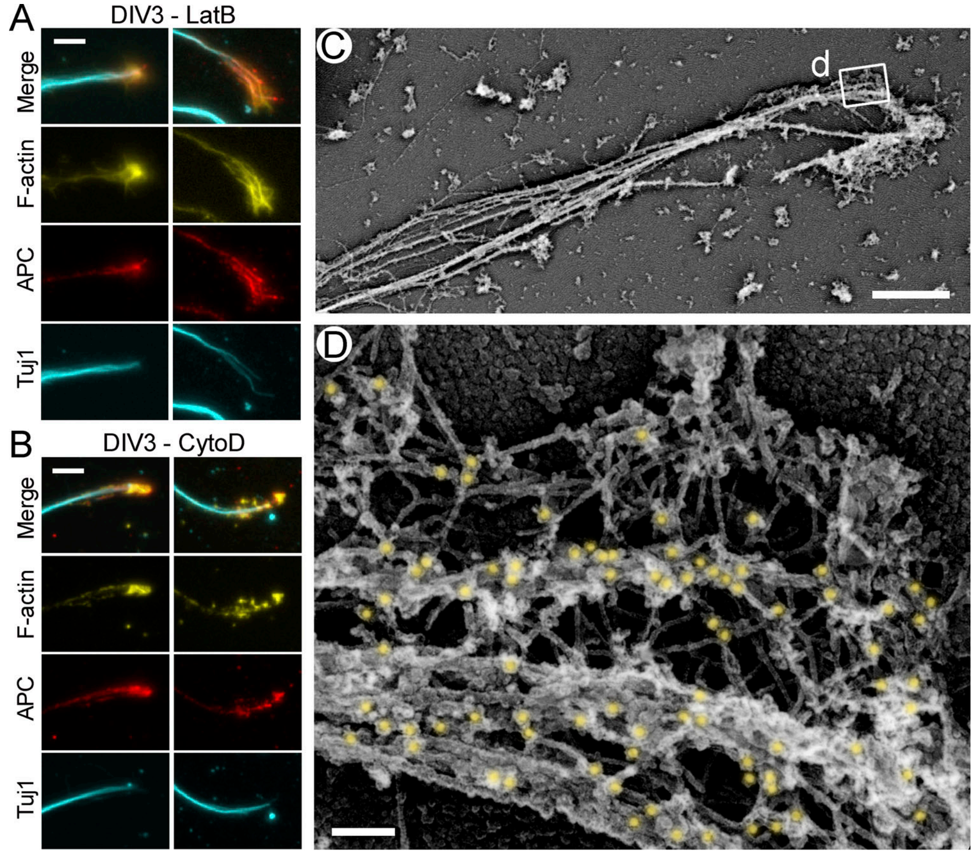

Figure S2. **Localization of APC in growth cones of rat hippocampal neurons treated with low concentrations of actin polymerization inhibitors. (A and B)** Fluorescence staining with phalloidin (F-actin) and antibodies to APC and βIII tubulin (Tuj1) of DIV3 neurons treated with 1 µM LatB (A) or 1 µM CytoD (B) for the last 24 h of culture. Two examples are shown in each case. **(C and D)** Immunogold PREM with APC antibody and 12-nm colloidal gold-conjugated secondary antibody of DIV2 neurons treated with 1 µM CytoD for the last 24 h of culture. Boxed region in C is enlarged in D. Gold particles are highlighted in yellow. Scale bars, 10 µm (A and B), 2 µm (C), and 100 nm (D).

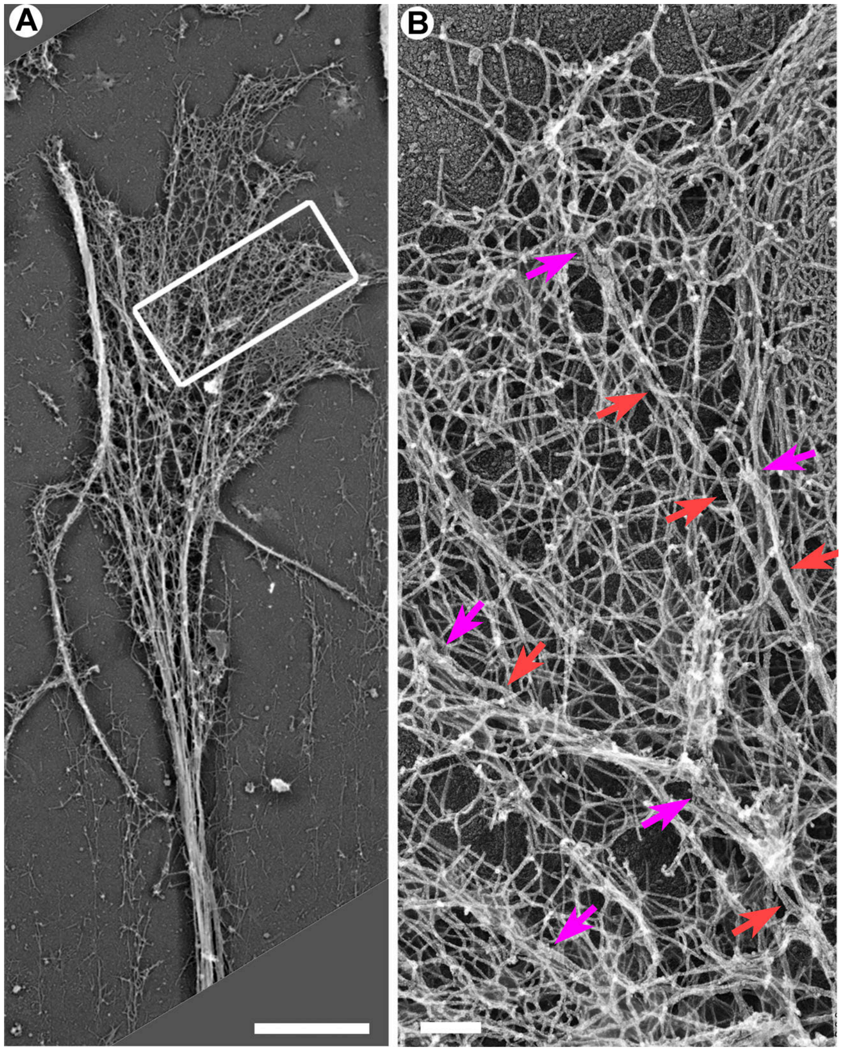

Figure S3. **PREM of a growth cone from a DIV14 hippocampal neuron stained with secondary 18-nm gold-conjugated anti-rabbit antibody without primary antibodies.** Boxed region in A is enlarged in B. No gold particles can be detected in these conditions confirming specificity of immunogold stainings. Red arrows indicate microtubules; magenta arrows indicate microtubule tips. Scale bars, 2 µm (A) and 200 nm (B).

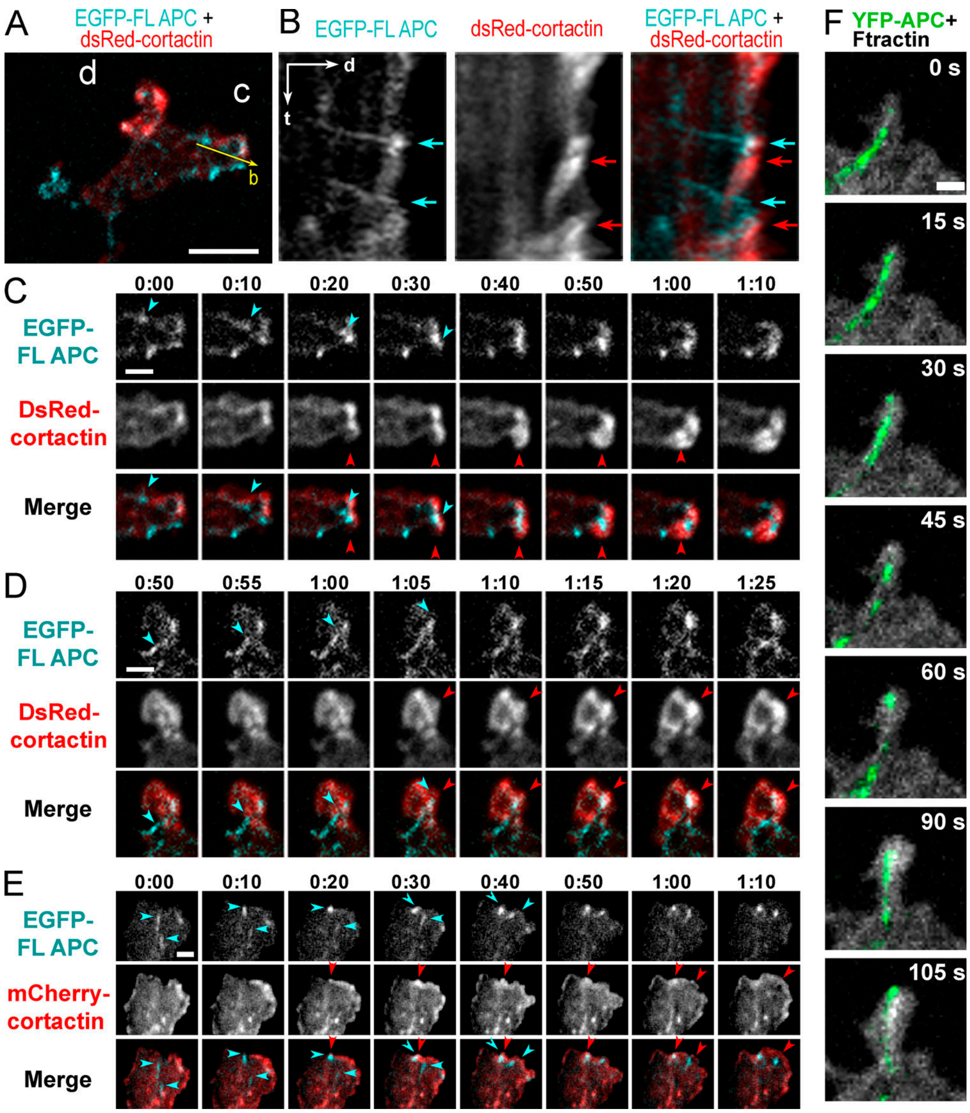

Figure S4. **Encounters of APC clusters with the cell edge correlate with transient actin-driven protrusions. (A)** Tip of the APC-induced process in a REF52 cell expressing EGFP-APC (cyan) together with dsRed-cortactin (red). Bar, 5 µm. **(B)** Kymograph taken along the yellow arrow in A shows APC tracks hitting the cell edge (cyan arrows) and cortactin-rich accumulations formed shortly after (red arrows). Time scale (t), 1 min; distance scale (d), 2 µm. **(C and D)** Frames from time-lapse sequences of the corresponding boxed regions in A. **(E)** Frames from time-lapse sequences of REF52 cell expressing EGFP-APC and mCherry-cortactin. Cyan arrows in C–E mark moving EGFP-APC clusters until they encounter the cell edge; red arrows mark subsequent enrichment of cortactin at the site of the encounter. Time is shown in min:s. Scale bars, 2 µm. **(F)** Frames from a time-lapse sequence of a COS7 cell expressing YFP-APC and mCherry-F-tractin. An entry of the APC-decorated microtubule tip into a small protrusion between 0 and 15 s is followed by accumulation of F-tractin starting from t = 30 s and expansion of the protrusion. Scale bar, 5 µm.

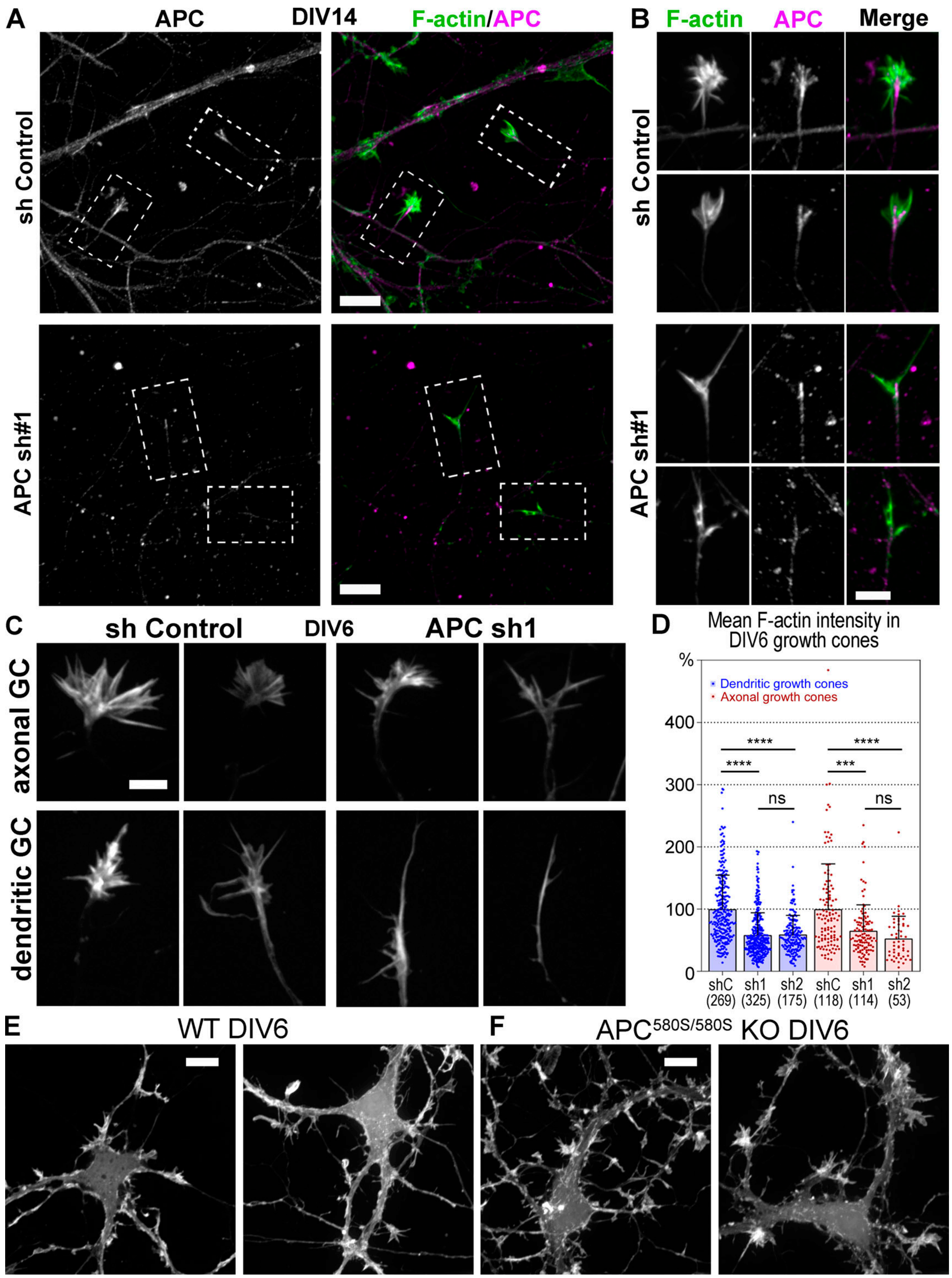

Figure S5. **Down-regulation of APC in hippocampal neurons. (A and B)** DIV14 rat hippocampal neurons treated with control (sh Control) or APC-targeting (APC sh1) shRNAs and stained with phalloidin and APC antibody. **(A)** Fluorescence intensities were adjusted identically in control (top) and APC shRNA-treated (bottom) images. **(B)** Enlarged boxed regions from A showing growth cones from control and APC-depleted neurons. The remaining growth cones in APC-depleted neurons are associated with low residual levels of APC. Fluorescence intensity of APC and phalloidin staining in growth cones of APC-depleted neurons (bottom panels) was adjusted to higher levels as compared with control growth cones (top panels) to show localization of the low remaining APC and F-actin signals. **(C)** Representative images of phalloidin-stained dendritic and axonal growth cones (GC) from DIV6 rat hippocampal neurons treated with control (sh Control) or APC-targeting (APC sh1) shRNAs. **(D)** Average fluorescence intensity of phalloidin staining in axonal and dendritic growth cones of control and APC-depleted rat hippocampal neurons at DIV6; mean ± SD; n is shown in parenthesis for each sample; ****, $P < 0.0001$; ***, $P < 0.001$; ns, not significant. Kruskal–Wallis multiple comparisons test with post hoc Dunn's test. **(E and F)** DIV6 mouse hippocampal neurons from wild-type (E) and floxed $APC^{580S/580S}$ mice (F). $APC^{580S/580S}$ neurons were transfected with Cre recombinase. Scale bars (apply to all images within indicated panels), 10 µm (A, E, and F) and 5 µm (B and C).

https://doi.org/10.1083/jcb.202003091

Video 1. **Dynamics of EGFP-FL APC and mCherry-F-tractin in REF52 cells.** Arrows indicate protrusion events occurring after an encounter of the APC-positive microtubule tips with the cell edge. The total length of the sequence is 10 min with 2-s intervals between frames. Scale bar, 2 µm.

Video 2. **Dynamics of EGFP-FL APC and dsRed-cortactin in REF52 cells.** Arrows indicate protrusion events occurring after an encounter of the APC-positive microtubule tips with the cell edge. The total length of the sequence is 5 min with 5-s intervals between frames. Scale bar, 3 µm.

Video 3. **Dynamics of EGFP-FL APC and dsRed-cortactin in REF52 cells.** Arrows indicate protrusion events occurring after an encounter of the APC-positive microtubule tips with the cell edge. The total length of the sequence is 24 min with 5-s intervals between frames. Scale bar, 3 µm.

Video 4. **Dynamics of EGFP-FL APC and mCherry-F-tractin in COS7 cells.** Arrows indicate protrusion events occurring after an encounter of the APC-positive microtubule tips with the cell edge. The total length of the sequence is 5 min with 5-s intervals between frames. Scale bar, 2 µm.

Video 5. **Dynamics of growth cones in control and APC-depleted neurons.** Time-lapse microscopy of DIV6 hippocampal neurons infected at DIV1 with lentiviruses carrying mCherry-F-tractin and either nontargeting (control) or APC-targeting (APCsh1) shRNA. Scale bar, 10 µm.

https://doi.org/10.1083/jcb.202003091